PHILOSOPHICAL TRANSACTIONS OF THE ROYAL SOCIETY A MATHEMATICAL, PHYSICAL & ENGINEERING SCIENCES

The Magnetoresistance of Polycrystalline Copper

Brian Pippard

Phil. Trans. R. Soc. Lond. A 1979 **291**, 569-598
doi: 10.1098/rsta.1979.0042

THE MAGNETORESISTANCE OF POLYCRYSTALLINE COPPER

By SIR BRIAN PIPPARD, F.R.S.

Cavendish Laboratory, Cambridge CB3 0HE, U.K.

(*Received* 16 *August* 1978)

CONTENTS

The effective medium theory has been applied to calculate the transverse magnetoresistance of random polycrystalline copper on the basis of the known Fermi surface, in order to explain the nearly linear variation of resistance with magnetic field up to very high values. Ziman's (1958) conjecture that the conductivity tensor should be averaged over all orientations is shown to be a good first approximation, though it does suggest that the resistance should have been observed to approach saturation in some experiments, when the open orbits might play a dominant role at large values of $\omega_c\tau$. The effective medium theory, by raising the saturation level considerably, eliminates this difficulty. The conductivity due to open and highly extended orbits, when calculated by geometrical analysis of the Fermi surface, is found to be quite sufficient to account for the observed behaviour. Certain residual discrepancies, especially a deficit in conductivity in very pure samples at large $\omega_c\tau$, are explained as arising partly from size effects and small angle scattering, but mainly from the markedly non-random texture of drawn and annealed wires; it is concluded that there is no reason to doubt that standard theories of magnetoresistance are capable of interpreting the observations. Most of the calculations of conductivity due to open and extended orbits are straightforward in principle and remarkably insensitive to the least well known parameters involved, the relaxation time and the angular distribution of scattering, so that the theoretical predictions are reasonably secure. Only in dealing with the extended orbits in the vicinity of high symmetry directions are approximations of dubious validity invoked, and even they are provided with more or less plausible justification. For the most part, however, the work represents a drawing together of well established concepts, and their application to a real Fermi surface rather than to convenient but imprecise approximate models.

Vol. 291. A 1385. 47 [Published 31 July 1979

Introduction

It was noted by Kapitza (1929) that the resistance of many metals in the form of polycrystalline wires increased in a transverse magnetic field according to an almost linear law. Not having access to liquid helium at the time, he was hardly able, even with his very strong impulsive fields, to attain values of $\omega_c\tau$ greater than unity (ω_c = cyclotron frequency, τ = relaxation time). The linear variation at such low values may be explained in terms of rather sharp edges, or narrow necks, on the Fermi surface which generate corresponding sharp corners in the orbits of electrons, allowing them to change direction in a small fraction of the cyclotron period, and causing the quadratic variation at low field strengths to give way to something close to linear (e.g. Pippard 1964). What is surprising about copper is that this linear variation persists up to very high values of $\omega_c\tau$, 200 or more, but only in polycrystals; single crystals show either saturation or a roughly quadratic increase at high fields, according to the orientation of $\boldsymbol{B}$ relative to the crystal axes. The general features of magnetoresistance in single crystals are well understood, the non-saturating pattern being ascribed to the presence of electrons in open or, at least, highly extended orbits. It has, however, remained in doubt whether in a polycrystal whose individual grains show saturation or quadratic behaviour, the average should automatically be roughly linear, or whether some other process must be postulated to explain the observations. Various attacks on the problem have established methods appropriate to a full analysis, and the most that can be claimed for the present work is that it has drawn on these existing techniques to carry through the analysis with sufficient (but not excessive) care to the point where it is highly arguable that nothing extra need be sought in explanation of the larger range of field strength over which the linear magnetoresistance persists. It will become clear in the final discussion that further elaboration of the theory to place this assertion beyond cavil would be exceedingly laborious.

Theoretical work started with the observation by Ziman (1958) that a Fermi surface consisting of non-intersecting cylinders lying along [111] directions would exhibit some important features of the copper Fermi surface, notably that section by planes normal to $\boldsymbol{B}$ would generate highly elongated orbits. The conductivity of such a system for arbitrary orientation of $\boldsymbol{B}$ is easy to calculate, and Ziman showed that if one simply averaged the conductivity over all orientations, $\overline{\sigma}_{xx}$ and $\overline{\sigma}_{xy}$ varied as $1/B$, $\boldsymbol{B}$ being taken to lie along the z-axis. If $\overline{\sigma}_{xz}$, $\overline{\sigma}_{yz}$, etc. vanish, the transverse resistivity is obtained by inverting the conductivity tensor:

$$\overline{\rho}_{xx} = \overline{\sigma}_{xx}/(\overline{\sigma}_{xx}^2+\overline{\sigma}_{xy}^2), \tag{1}$$

and clearly in this case $\overline{\rho}_{xx}$ has the desired variation proportional to B. Ziman made no claim to have demonstrated the correctness of this averaging procedure, but a plausible (though ultimately untenable) case may be argued in the following terms. As B is increased, $\overline{\sigma}_{zz}$ remains high while in most crystallites $\overline{\sigma}_{xx}$ and $\overline{\sigma}_{xy}$ fall to low values; it is therefore to be expected that, whatever the pattern of current flow, E_z will be much smaller than E_x or E_y. If we may take E_z as zero, it follows from the irrotational nature of $\boldsymbol{E}$ that $\partial E_x/\partial z = \partial E_y/\partial z = 0$. Now the absence of any variation of the transverse components of $\boldsymbol{E}$ with z in a polycrystalline medium can only be understood as an indifference of $\boldsymbol{E}$ to the granularity; $\boldsymbol{E}$ is the same in each grain and consequently the mean value of the current density is given by the average conductivity:

$$\overline{\sigma}_{ij} = \langle\sigma_{ij}\rangle, \tag{2}$$

the bar being used to denote the observable value for the polycrystalline mass, the angular brackets denoting the average over all crystal orientations.

The mechanism underlying Ziman's conjecture (2) is that the same $\boldsymbol{E}$ sets up in each grain whatever current the local conductivity demands, and that the discontinuities in the normal components of $\boldsymbol{J}$ at grain boundaries are responsible for generating currents that flow parallel to $\boldsymbol{B}$. The assumption, however, that these parallel currents are non-dissipative will not stand up, and this is where Ziman's conjecture fails. Imagine a line drawn parallel to $\boldsymbol{B}$ through the sample, intersecting many grain boundaries, at each of which a current is generated, sometimes positive, sometimes negative, with mean value zero. The dissipation due to J_z at any point is $\rho_{zz}J_z^2$, or $\rho_{zz}N\overline{j_z^2}$ where $\overline{j_z^2}$ is the mean square value of J_z generated at a grain boundary and N is the number of grain boundaries intersected by the lines. Unfortunately as the size of the sample, and hence N, is increased this diverges, and it is invalid to assume that dissipation due to J_z is negligible. Although this argument destroys any hope of a really simple treatment along Ziman's lines, it will be appreciated that the divergence just revealed is itself the artefact of an oversimplification. The current jets streaming along the z-direction from each grain boundary do not continue for ever, but gradually spread out to merge with, and help to cancel, other current jets. The lateral spread is, however, slow (Herring 1960), and it is not until one moves along $\boldsymbol{B}$ for a distance about $(\overline{\sigma}_{zz}/\overline{\sigma}_{xx})^{\frac{1}{2}}$ as large as a crystallite diameter that one finds any significant merging of currents from the two sides of a crystallite. It is a highly convenient consequence of this that a given jet must traverse many neighbouring crystallites before being dissipated, and it is likely to be a very adequate assumption that the current flow in the vicinity of a given crystallite is much the same as if it were embedded in a uniform medium having the average properties exhibited by the polycrystal. This is precisely the model commonly referred to as the effective medium approximation, whose history and bibliography is very fully dealt with by Landauer (1978). It has been found successful in applications even where the additional advantage of current jetting is absent, and there is little doubt of its legitimacy in the present application. The details of the theory have been presented on several occasions (Stachowiak 1970, Stroud 1975) but not in a form that reveals readily how to use it in numerical work, as is the aim of the next section.

Effective medium approximation

The essence of this approximation is that each crystallite may be regarded as a spherical inclusion in a uniform medium having the properties that would be determined by measurements on a polycrystalline aggregate. A field E_i applied to the sample generates a current density J_i in the inclusion, whose magnitude and direction are determined by the conductivity tensors of medium $(\overline{\sigma}_{ij})$ and inclusion (σ_{ij}). For any arbitrary choice of $\overline{\sigma}_{ij}$ and a given distribution function of σ_{ij} for differently oriented crystallites, the mean current, averaged evenly over all crystallite orientations, is not in general equal to $\overline{\sigma}_{ij}E_j$, and the problem is to find $\overline{\sigma}_{ij}$ such that this is the case. Because $\overline{\sigma}_{ij}$ refers to a random polycrystal, its form is restricted by symmetry considerations; if $\boldsymbol{B}$ lies along the z-direction, $\overline{\sigma}_{xx} = \overline{\sigma}_{yy} \neq \overline{\sigma}_{zz}$, $\overline{\sigma}_{yx} = -\overline{\sigma}_{xy}$, and all other components vanish. In the individual crystallite no such restrictions apply, but we shall assume that cross terms involving z, e.g. σ_{xz}, are negligible.

The requirements that curl $\boldsymbol{E}$ and div $\boldsymbol{J}$ both vanish imply that in the medium the potential ϕ obeys the modified Laplace equation, $\phi_{xx}+\phi_{yy}+r^2\phi_{zz} = 0$, where $r^2 = \overline{\sigma}_{zz}/\overline{\sigma}_{xx}$, and may be between 5 and 50 in the applications treated here. By introducing a scaled coordinate system in which all z-dimensions are reduced by a factor r, the equation may be converted into Laplace's, while in this process the spherical inclusion becomes an oblate spheroid (discus) with axial

ratio r. A uniform electric field applied in the plane of the discus, the x, y plane normal to $\boldsymbol{B}$, polarizes the inclusion uniformly and generates a uniform field within it, also in the x, y plane, which in the absence from σ_{ij} of cross terms involving z sets up a current also lying in this plane. It is now necessary to ensure continuity of current across the interface, and we shall concentrate on the equatorial plane of the discus in the knowledge that if all goes well here the rest follows automatically.

If the polarization vector within the discus is P_i, and the uniform applied field is E_i, the internal field is $E_i - DP_i/\epsilon_0$, where D is the depolarizing coefficient for a spheroid of axial ratio r (Stratton 1941, p. 214):

$$D = \tfrac{1}{2}[r \arctan (r-1)^{\frac{1}{2}}/(r-1)^{\frac{3}{2}} - 1/(r-1)]. \tag{3}$$

At a point in the equatorial plane where the normal to the surface is defined by the unit vector n_i the surface charge density is $n_i P_i$ (repeated indices imply summation over x and y only), and therefore the field just outside the discus is given by $E_i - DP_i/\epsilon_0 + n_i(n_k P_k)/\epsilon_0$. Continuity of the normal component of current then demands that

$$n_j[\sigma_{ji}(E_i - DP_i/\epsilon_0) - \overline{\sigma}_{ji}(E_i - DP_i/\epsilon_0 + n_i n_k P_k/\epsilon_0)] = 0$$

at all points on the equator. The form of $\overline{\sigma}_{ji}$ enables this to be written

$$n_j[(\sigma_{ji} - \overline{\sigma}_{ji})(E_i - DP_i/\epsilon_0) - \overline{\sigma}_{xx} P_j/\epsilon_0] = 0,$$

and the vanishing of the quantity in square brackets assures the satisfying of the boundary condition. Hence if β_{ij} is the inverse of the tensor $(\sigma_{ij} - \overline{\sigma}_{ij})\, D + \overline{\sigma}_{xx}\delta_{ij}$, then

$$P_k = \epsilon_0 \beta_{kj}(\sigma_{ji} - \overline{\sigma}_{ji})\, E_i.$$

Given the polarization, the electric fields and currents follow automatically, and the condition that the average current density in a crystallite shall be $\overline{\sigma}_{ij} E_j$ takes the form

$$\langle \sigma_{ij} \beta_{jk} \rangle = \overline{\sigma}_{ik}/\overline{\sigma}_{xx}. \tag{4}$$

This equation, whose solution determines the properties of the polycrystal, takes the form of two simultaneous equations for the unknown $\overline{\sigma}_{xx}$ and $\overline{\sigma}_{xy}$:

$$\langle [\sigma_{xx}(\overline{\sigma}_{xx} + \lambda\sigma_{yy}) - \lambda\sigma_{xy}(\sigma_{yx} - \overline{\sigma}_{yx})]/M \rangle = 1/(1+\lambda), \tag{5}$$

and

$$\langle (\lambda\overline{\sigma}_{xy}\sigma_{xx} + \overline{\sigma}_{xx}\sigma_{xy})/M \rangle = \overline{\sigma}_{xy}/(1+\lambda)\,\overline{\sigma}_{xx}, \tag{6}$$

in which

$$\lambda = D/(1-D) \quad \text{and} \quad M = (\overline{\sigma}_{xx} + \lambda\sigma_{xx})(\overline{\sigma}_{xx} + \lambda\sigma_{yy}) + \lambda^2(\sigma_{xy} - \overline{\sigma}_{xy})^2. \tag{7}$$

In the present application the second term in M may be dropped without significant error, since λ is typically less than 0.15 and $\sigma_{xy} - \overline{\sigma}_{xy} < \frac{1}{5}\overline{\sigma}_{xx}$. Larger errors than this are incurred elsewhere in the calculations. A more significant simplification, and one that does not involve approximation, reduces the degrees of freedom involved in averaging over all orientations. Rotation of a crystallite about $\boldsymbol{B}$, $\boldsymbol{E}$ being fixed, is equivalent to keeping the crystallite at rest while rotating $\boldsymbol{E}$ about $\boldsymbol{B}$ as axis. Now the transverse elements of σ_{ij} are liable to be highly anisotropic, since the important crystallites are those supporting highly extended or open orbits. The same applies to the tensor σ'_{ij}, specifying the current set up within any crystallite by application of the external field E_i. Now there will be two orthogonal principal directions for E_i with respect to which $\sigma'_{xy} = -\sigma'_{yx}$, only the Hall terms being present in the off diagonal elements. If the diagonal elements are then σ'_1 and σ'_2, it is easy to show that the mean current, averaged over

all directions of E_i in the plane normal to $\boldsymbol{B}$, is $\frac{1}{2}(\sigma_1'+\sigma_2')\,E$ parallel to E_i and $\sigma_{xy}'E$ normal to E_i. Thus instead of averaging over all directions of E_i for each orientation of $\boldsymbol{B}$ in the crystal lattice, it is sufficient to take the mean of the contributions of the two principal directions, and ignore all but the Hall contribution to the off-diagonal elements. Moreover, since the important crystallites are those carrying extended orbits, for which σ_1 may be taken as much greater than σ_2, no serious error arises from assuming σ_2 to vanish. With these simplifications (5) and (6) take the following form:

$$\tfrac{1}{2}P_{xx}+\lambda[\overline{\sigma}_{xy}P_{xy}-\overline{\sigma}_{xy}^2(1-\lambda P_{xx})/\overline{\sigma}_{xx}+Q_{xy}]/\overline{\sigma}_{xx}=1(1+\lambda), \tag{8}$$

and

$$P_{xy}=\overline{\sigma}_{xy}[1/(1+\lambda)-\tfrac{1}{2}\lambda P_{xx}]/\overline{\sigma}_{xx}, \tag{9}$$

in which

$$P_{xx}=\langle\sigma_1/(\overline{\sigma}_{xx}+\lambda\sigma_1)\rangle,$$

$$P_{xy}=\langle\sigma_{xy}/(\overline{\sigma}_{xx}+\lambda\sigma_1)\rangle,$$

and

$$Q_{xy}=\langle(\sigma_{xy}-\overline{\sigma}_{xy})^2/(\overline{\sigma}_{xx}+\lambda\sigma_1)\rangle.$$

In deriving (9), use is made of the relation $\langle 1/(\overline{\sigma}_{xx}+\lambda\sigma_1)\rangle=(1-\lambda P_{xx})/\overline{\sigma}_{xx}$. It is worth remarking in this connection that although it enables P_{xx} to be evaluated either as $\langle\sigma_1/(\overline{\sigma}_{xx}+\lambda\sigma_1)\rangle$ or by way of $\langle 1/(\overline{\sigma}_{xx}+\lambda\sigma_1)\rangle$, the former is preferable, in that it is an average which is dominated by those crystallites having high values of σ_1; it will become apparent that these relatively rare crystallites can be enumerated with much greater ease than the more common type with lower conductivity.

The problem of solving (8) and (9) may now be expressed in terms of finding $\overline{\sigma}_{xx}$ and $\overline{\sigma}_{xy}$ such that

$$P_{xx}=2/(1+\lambda)-2\lambda(Q_{xy}/\overline{\sigma}_{xx})/(1+\lambda^2\overline{\sigma}_{xy}^2/\overline{\sigma}_{xx}^2). \tag{10}$$

Since the second term is itself very small, and $\overline{\sigma}_{xy}$ occurs only there, and then as a second order correction, a good start to the solution involves finding $\overline{\sigma}_{xx}$ such that

$$P_{xx}=2/(1+\lambda), \tag{11}$$

and proceeding by substituting this in (9) to determine $\overline{\sigma}_{xy}$ in the form:

$$\overline{\sigma}_{xy}=\frac{1+\lambda}{1-\lambda}P_{xy}\overline{\sigma}_{xx}=\sigma_{\mathrm{H}}-\frac{1+\lambda}{1-\lambda}\overline{\sigma}_{xx}\Delta P_{xy}, \tag{12}$$

in which ΔP_{xy} is derived from the Hall deficit, $\Delta\sigma_{xy}$, defined as $\sigma_{\mathrm{H}}-\sigma_{xy}$, where σ_{H} is the Hall conductivity (ne/B) expected if all the conduction electrons were to move in closed electron-like orbits. Thus

$$\Delta P_{xy}\equiv\langle\Delta\sigma_{xy}/(\overline{\sigma}_{xx}+\lambda\sigma_1)\rangle.$$

Then the transverse resistivity $\overline{\rho}_{xx}$ follows immediately from (1). It is easy enough to correct this answer for neglect of the second term in (10), but since even in the worst case treated here the correction changes $\overline{\rho}_{xx}$ by only 1 % we shall not trouble to do so.

The approximation involved in Ziman's conjecture (2) is now clear: λ must be small enough to be dropped in the evaluation of P_{xx}. In the present application, however, $\sigma_1/\overline{\sigma}_{xx}$ is as large as 5 for a significant proportion of the crystallites that matter, so that λ must be much less than 0.1 before a straight average of σ_1 can be tolerated. Values of $\overline{\sigma}_{zz}/\overline{\sigma}_{xx}$ well over 100 are needed, and no experiment yet performed attains the required conditions. Nevertheless, Ziman's conjecture leads to results that are not wildly astray, and it serves a useful purpose in indicating, as will appear later, which factors are of minor importance.

Calculation of conductivity: introduction

It is now necessary to derive expressions for σ_{ij} in those crystallites that contribute most to P_{xx} and ΔP_{xy}, and we must start with an overall categorization of the orbits in which electrons can move. This is the point of departure from the analyses of Ziman and of Stachowiak (1970, 1973) who applied their arguments to simplified models of the Fermi surface of copper, thereby considerably underestimating the prevalence of open and extended orbits, which are of the highest importance. Since the form of the Fermi surface is known with considerable precision we shall work from this, using Halse's (1969) determination or, where convenient, the tabulations of Powell (1966) which, though not so well based, are good enough for the present purpose. The periodically extended Fermi surface forms a body-centred cubic array of near-spheres connected by necks aligned along body diagonals. The centres of the necks themselves form a simple cubic lattice whose basis will be taken as the unit of length in k space; since the unit cube holds half an electron per atom, the free-electron sphere for copper has volume 2 and radius 0.7816. Except for those special directions of $\boldsymbol{B}$ whose direction cosines are rationally related, a section of this extended surface by a plane normal to $\boldsymbol{B}$ cuts each repetition of the primitive Fermi surface at a different level; the orbits revealed by this section reproduce in their frequency of occurrence the orbits executed by electrons in the field $\boldsymbol{B}$. It is convenient to imagine a thin plane section, of thickness δ, cut from the extended surface; an area $4/\delta$ then holds 2 electrons per atom and defines a volume equal to the Brillouin zone. By enumerating the orbits of a given type lying within this area, and ascribing to each its conductivity, a correct measure of σ_{ij} is obtained for this orientation of $\boldsymbol{B}$.

The general principles governing the character of the orbits were first enunciated by Lifshitz & Peschanskii (1958). When $\boldsymbol{B}$ lies close to a high-symmetry direction, the normal plane cuts through the belly of the Fermi surface in some places, generating simple electron orbits, and through four necks in others, generating simple hole orbits. The regions of electron and hole orbits are separated by an aperiodic open orbit whose general direction is the line of intersection of the plane normal to $\boldsymbol{B}$ and the nearest high-symmetry plane. Thus, as $\boldsymbol{B}$ is tilted away from [100], the possibility disappears of cutting four necks to generate a hole orbit, and simultaneously the open orbits vanish. Instead there are left highly extended, but finite, orbits, whose length steadily decreases as $\boldsymbol{B}$ is moved further away from [100]. Similar behaviour occurs around [110] and [111], and the characteristics of the pattern are summed up in figure 1, which shows on a stereographic projection the basic $\frac{1}{48}$ of the solid angle enclosed in the spherical triangle defined by the three principal symmetry directions. The boundaries of the triangle, where the direction cosines cannot be entirely irrational, need special treatment and are the sites of periodic open orbits on either side of which lie extended orbits; there is also a line GH of periodic open orbits, flanked by extended orbits, running through the triangle and defined by a (111) plane.

To proceed to a more quantitative treatment, it is convenient to treat the three principal symmetry directions separately, though the same process will comprehend [100] and [110] together, leaving [111] for special attention. Figure 2 shows a plane section normal to [110] with the Fermi surface section in two cells, but the rest of the periodically extended structure represented by the rectangular lattice of neck centres; the (110) section has $k_1 = \sqrt{2}$, $k_2 = 1$ and successive layers of neck centres are spaced k_3 apart, with k_3 equal to $\sqrt{2}$. Only half the necks appear; the rest can indeed generate hole and open orbits – the 'lemons' described by Halse (1969) – but in such small amount that we shall neglect them. A similar diagram serves for the

(100) plane section except that now $k_1 = k_2 = k_3 = 1$ and all necks are involved; the Fermi surface section in this case is also shown in figure 2. Now a plane normal to $\boldsymbol{B}$ (which we shall refer to as a B plane) can be represented on this diagram by contour lines showing where the B plane cuts each successive layer of neck-centres. If the orientation of $\boldsymbol{B}$ is defined by (θ, ϕ) as in figure 1, the contours are set at ϕ, as shown in figure 2, with a spacing of $k_3 \cot\theta$. Wherever a

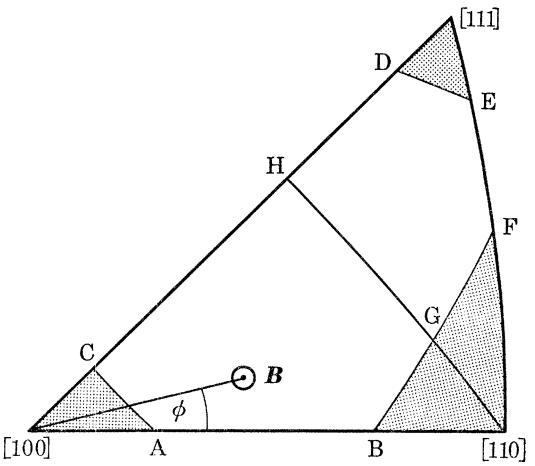

FIGURE 1. Basic unit of stereographic projection, showing (shaded) the directions of $\boldsymbol{B}$ for which aperiodic open orbits exist.

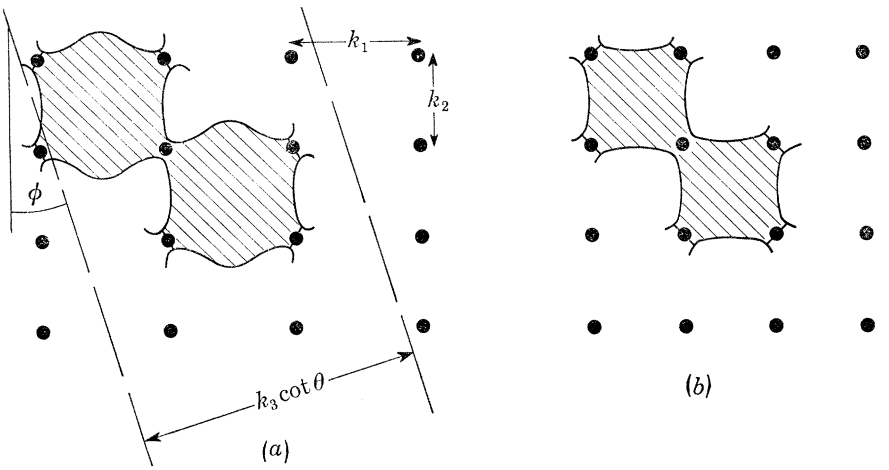

FIGURE 2. Sections of periodically extended Fermi surface by (*a*) [110] plane and (*b*) [100] plane. Only two replications of the section are shown in each case, together with the lattice formed by the centres of the necks.

contour passes through a lattice point, the B plane cuts through the very centre of a neck, as does L in figure 3, and the electron, passing from one cell of the periodic pattern to the next, executes an orbit that extends over at least two repetitions of the Fermi surface, and more if more necks are cut by the B plane. A contour passing close to a lattice point may still cut the neck and enable the electron to pass to the neighbouring cell; but a plane such as N, lying outside the limits MM′, misses the neck and the electron carries on past it, executing a belly orbit all in one cell.

The pattern may be schematized as in figure 4(*a*). The section of the Fermi surface through the necks is represented by a rectangle, so that the filled regions of periodically extended k space on

this plane section appear as shaded areas of a chessboard. An electron is impelled by $\boldsymbol{B}$ along a line of the pattern, and at each intersection it turns right, following round a shaded area, if its B plane does not cut that neck, and left, following round an unshaded area, if it does. To indicate which necks are cut we draw horizontal lines (P lines) of length $2P(P \equiv p \operatorname{cosec}\theta \sec\phi)$ centred on

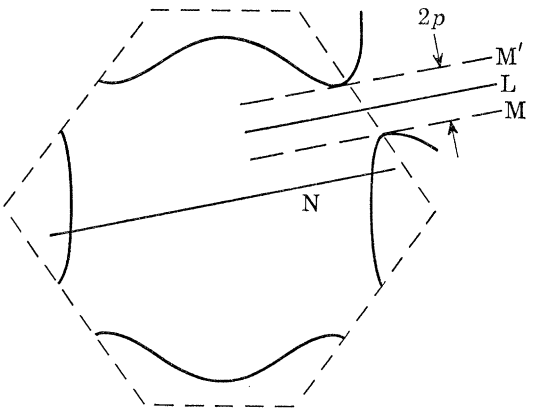

FIGURE 3. Sections of the Fermi surface by planes whose normal lies in the plane of the diagram.

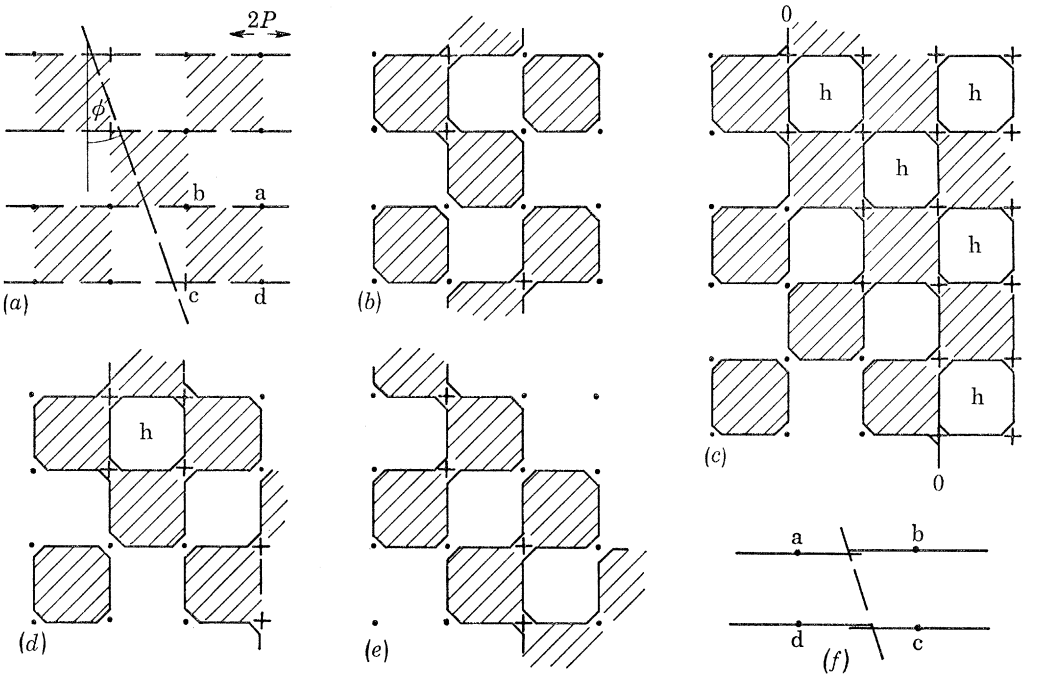

FIGURE 4. Schematic representation of various types of orbit. Hole orbits are labelled h. For further explanation see text.

each lattice point. It follows from the definition of p in figure 3 that the neck is cut if the contour cuts the P line. It should be noted that the necks are not in general equivalent and that, for example, there are four different values of P for the orientations around [100], and two different values around [110].

A typical contour is drawn in figure 4 (a) and each cut neck marked with a cross. The pattern

of crosses is transferred to figure 4 (*b*) and the orbits drawn by following the rule given in the last paragraph. It is helpful to realize that the pattern of crosses is always compact, in the sense that along any line the crosses belonging to a given contour form a continuous sequence, without gaps. This ensures that any space between open orbits is filled with hole orbits, as in 4 (*c*), and that those hole orbits are always simple, never extended. A pattern like that in 4 (*d*) is precluded by the requirement of compactness, and it may be verified by attempting to construct counter examples that a hole orbit cannot be enclosed within an extended orbit. As ϕ is increased, the open orbits draw closer and contain less hole orbits until in the end they contain none. At the very point where

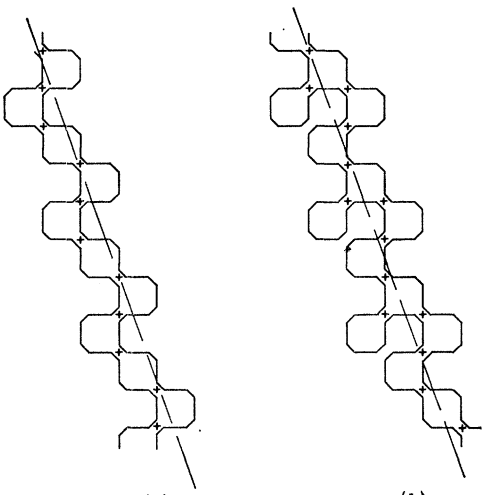

FIGURE 5. Illustrating sinuosity, γ. In (*a*) $\gamma = 1$, in (*b*) γ is close to $\frac{4}{3}$.

it is no longer possible to produce the four crosses on a square needed to define a hole orbit, the possibility arises of the contour missing both the top right and the bottom left corners of what would otherwise be a hole orbit, as in 4(*e*). When this happens the orbit terminates. Since in irrational directions the ***B*** contour runs through every point in the unit cell, the disappearance of the last hole orbit automatically signals the end of the open orbits also. Hence if the four necks which in principle are different are labelled as in 4 (*f*), the boundary of the open orbit region is defined by the condition:

$$P_{\mathrm{b}} + P_{\mathrm{d}} = k_1 + k_2 \tan\phi. \tag{13}$$

It is quite a good approximation to take $P_{\mathrm{b}} + P_{\mathrm{d}}$ as $2p_0/\theta\cos\phi$, where p_0 is the value of p for B planes normal to the symmetry axis itself, i.e. 0.108 for [100] and 0.147 for [110]. Then for example, the value of θ at the boundary around [100] is roughly given by the expression $\theta_0 = 0.1524\sec(\phi - \frac{1}{4}\pi)$. Similar approximations apply to the other symmetry directions and, although they are not normally used in the actual computations, they serve to explain why the boundary lines shown in figure 1 are very nearly straight.

The direction in which the spine of a highly extended orbit lies is clearly the line of the B contour, and the quantity $k_{\parallel}$, defined as the unit length measured along the spine, is $k_2\sec\phi$. It is also necessary to introduce the idea of sinuosity. The most economical orbit running in a given direction, ϕ, is a simple chain without side arms, as in figure 5 (*a*); on each row of the lattice there

is one cross only, and the number of units making up the chain is just the number of rows it covers. Now each extra cross, lying as it must next to an existing cross, adds one more unit to the chain, as a side arm. It follows that the sinuosity, γ, defined as the ratio of the actual number of units in a chain of given overall length to the minimum needed, takes the same value for a long chain as the average number of crosses per line, which is $(P_a+P_b+P_c+P_d)/2k_1$. Since P_a+P_c is always very close to P_b+P_d, a good approximation follows from (13) for the open orbits at the boundary and the highly extended orbits just outside,

$$\gamma = 1+(k_2/k_1)\tan\phi. \tag{14}$$

Near [100], when $\phi = 20°$, $\gamma = 1.36$, and this case is illustrated in figure 5 (*b*).

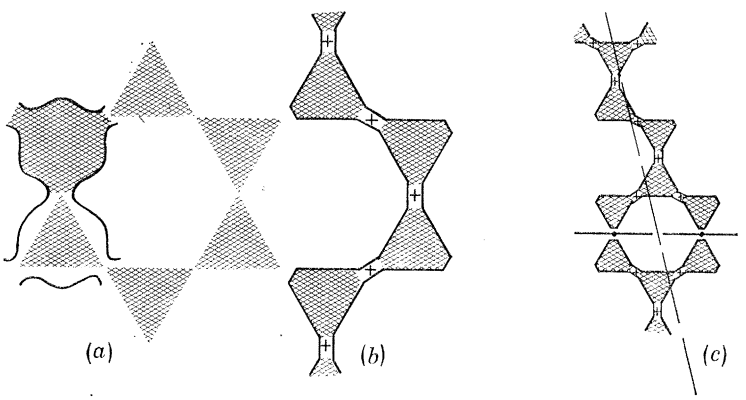

FIGURE 6. Sections of periodically extended Fermi surface in the vicinity of [111]. In (*a*) only one actual section is shaded, and the rest are schematized as in figure 4; (*b*) is an ideal orbit having $\gamma = 1$, while (*c*) shows a typical normal form with $\gamma = \frac{3}{2}$, and the termination of an extended orbit.

Around [111] a modified pattern obtains, the relevant lattice of neck centres having the hexagonal structure shown in figure 6, with a neck spacing of $\sqrt{2}$, and a layer spacing k_3 of $1/\sqrt{3}$. The hole orbits are hexagonal and exist only so long as the P lines on opposite sides of the hexagon meet. The most economical open orbit is produced by a chain of triangles, when there is one cross per row, and as with the other directions γ is the average number of crosses per row. At the boundary of the open orbit zone $P = \sqrt{2}$ and the normal pattern of crosses is an alternation of one and two per row, giving a value of $\frac{3}{2}$ to γ.

At this point, before proceeding to the detailed enumeration of orbits, it is convenient to break off the argument to derive certain results that will be required later.

THE FERMI SURFACE AND THE VALUE OF p

In Halse's (1969) representation of the Fermi surface of copper the necks are remarkably close in form to hyperboloids of revolution with [111] as axes. A (110) section is shown in figure 7 together with points lying on the hyperboloid

$$46(x^2+y^2)-116.5z^2 = 1. \tag{15}$$

When $\boldsymbol{B}$ lies 9° from [100] the $\boldsymbol{B}$ planes that just cut the neck lie as shown, $2p$ part. This case is almost the worst encountered, in the sense that the tangent points of almost all other $\boldsymbol{B}$ planes of importance lie even closer to the x, y plane. The hyperbolic approximation is clearly very good

for the present purpose. It is a simple exercise in coordinate geometry to show from (15) that if ϵ is the angle between $\boldsymbol{B}$ and the axis of the neck, then

$$p = 0.1474(1 - 1.395\cos^2\epsilon)^{\frac{1}{2}}. \tag{16}$$

For $\boldsymbol{B}$ near [100], θ and ϕ being defined as in figure 1,

$$\cos\epsilon = (\tfrac{2}{3})^{\frac{1}{2}}\sin\theta\cos(\phi_0 - \phi) + (\tfrac{1}{3})^{\frac{1}{2}}\cos\theta, \tag{17}$$

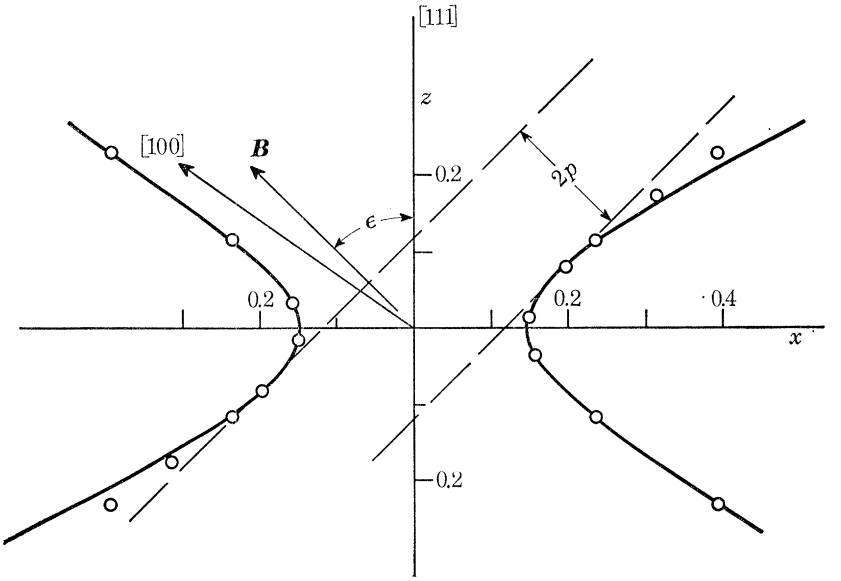

FIGURE 7. Geometry of a neck section, treated as a figure of revolution about the vertical [111] axis.

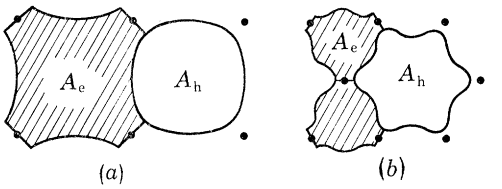

FIGURE 8. Electron and hole orbit areas; (*a*) for [100] and [110] sections, (*b*) for [111] section.

with ϕ_0 taking the values $\frac{1}{4}\pi$, $\frac{3}{4}\pi$, $\frac{5}{4}\pi$ and $\frac{7}{4}\pi$ for necks a, b, c and d. For $\boldsymbol{B}$ near [110], the necks that matter have axes normal to [110] and nearly normal to $\boldsymbol{B}$. If ϕ is measured from the (100) plane and θ from the [110] axis, then

$$\cos\epsilon = \sin\theta\cos(\phi_0 \pm \phi), \tag{18}$$

with $\cot\phi_0$ equal to $\sqrt{2}$, and the positive sign applying to necks b and d, the negative to a and c. For $\boldsymbol{B}$ near [111], ϕ is measured from a (110) plane and

$$\cos\epsilon = \tfrac{\sqrt{8}}{3}\sin\theta\cos(\phi_0 - \phi) + \tfrac{1}{3}\cos\theta, \tag{19}$$

where $\phi_0 = 0$ or $\pm\frac{2}{3}\pi$.

Also required are the areas of various orbits since, as will be seen, they play a part in determining the Hall deficit, $\Delta\sigma_{xy}$. Since this is usually rather small, great accuracy is not needed, and the areas have been found by drawing sections and counting squares. The tabulations of Powell

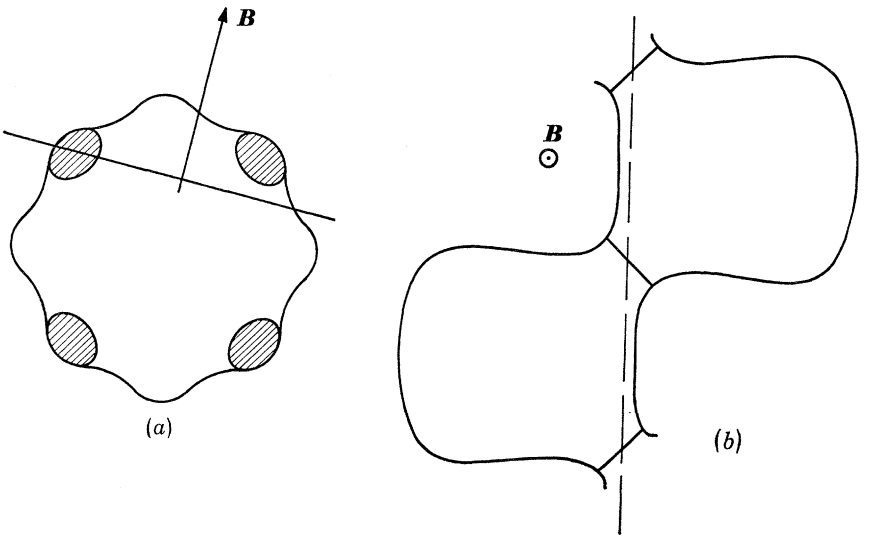

FIGURE 9. Periodic open orbit; (*a*) section of Fermi surface by plane normal to ***B***, (*b*) orbits in the *B* plane divided into identical units.

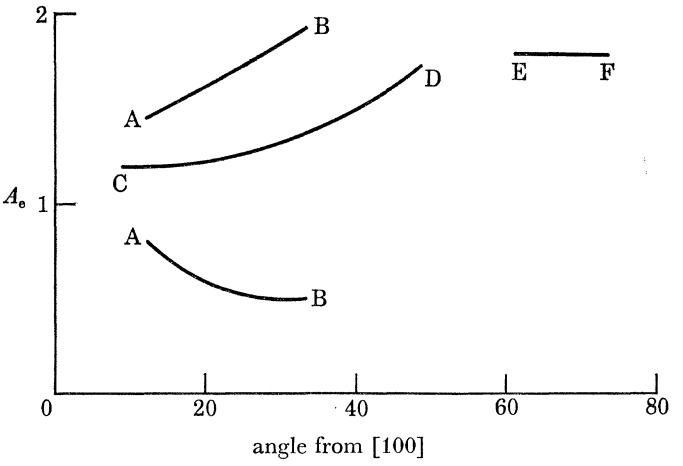

FIGURE 10. Variation with field direction of A_e, the unit area of periodic open orbits. Note that there are two different open orbits in the (110) plane. The letters relate to figure 1.

(1966) have been particularly valuable here. For neck sections in symmetry directions the areas are defined as in figure 8. It matters little in an extended or open orbit how many of the necks of the shaded electron orbit represent connections in the chain and how many are not cut: the area A_e as shown is accurate enough for both. The corresponding hole orbit has area A_h, and since the whole plane may be tesselated by use of both it is easy to see that

$$\left.\begin{aligned} A_e + A_h &= 2 \text{ for a [100] section and } 2\sqrt{2} \text{ for a [110] section,} \\ \text{and} \qquad 2A_e + A_h &= 4\sqrt{3} \text{ for a [111] section.} \end{aligned}\right\} \tag{20}$$

The actual magnitudes are as follows:

$$\left.\begin{aligned} &[100]: A_e = 1.22, \quad A_h = 0.78, \\ &[110]: A_e = 2.05, \quad A_h = 0.78, \\ &[111]: A_e = 1.71, \quad A_h = 3.51. \end{aligned}\right\} \tag{21}$$

When $\boldsymbol{B}$ lies in a symmetry plane so that the B plane generates periodic open orbits by cutting two necks, as for example in figure 9, the area of each unit in the resulting chain varies with θ and must be known, though again with no great accuracy, for $\Delta\sigma_{xy}$. For $\boldsymbol{B}$ lying in the two planes (100) and (110) the variation of A_e over the angular ranges needed is shown in figure 10; in the (111) plane the range of θ is small and A_e is very nearly constant at a value of 1.89.

Conductivity due to extended and open orbits

Stachowiak (1971) has given an expression for the conductivity along an extended orbit, and in this section his result is shown to be more generally valid than his model suggests, and the Hall conductivity is also derived. A convenient starting point is the expression for σ_{ij} in terms of the effective path L_i (Pippard 1968); if $\mathrm{d}S_j$ is an element of the Fermi surface, and if an electron at this point travels on the average a vector distance L_i before its motion is randomized by collisions, then

$$\sigma_{ij} = (e^2/4\pi^3\hbar) \oint L_i \,\mathrm{d}S_j. \tag{22}$$

This expression is valid in the presence of a uniform magnetic field.

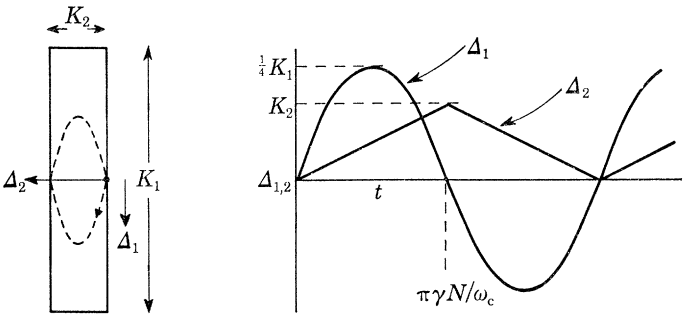

Figure 11. Illustrating calculation of extended orbit conductivity.

It should be noted that until the very end of this section conventional units are used for k space. When section of the Fermi surface by a B plane generates an extended orbit, a typical electron moves round the orbit at a more or less regular speed in k space, taking time $2\pi/\omega_c$ to accomplish each unit in the chain. In real space it describes a similar orbit so far as the projection on a plane normal to $\boldsymbol{B}$ is concerned, but scaled by a factor $\hbar/eB$. When the orbit is highly extended the fine details of its motion are of little consequence compared with the general motion, and it is legitimate to replace the real orbit by a thin rectangle of the same length, provided allowance is made for sinuosity. Thus an extended orbit which in its most economical form would consist of N simple orbits linked in a chain, but with $(\gamma-1)N$ extra units attached roughly evenly along it, would be replaced by a rectangle of the same overall length, K_1, around which the electrons would travel at such a speed as to cause them to make a complete circuit in time $2\pi\gamma N/\omega_c$. The width, K_2, of the rectangle should be chosen so that the area K_1K_2 is the same as that of the real orbit, i.e. γNA_e; this choice of K_2 ensures that the high-field limit of σ_{xy} is correctly derived.

We evaluate (22) by first finding the average value of L_j for electrons on one long side of the rectangle. Imagine a cluster of electrons evenly distributed along the side, and moving steadily around it, so that the path of the centroid, as a function of time, is a succession of parabolas for movement along the length, and a sawtooth for movement across the width, as shown in figure 11.

In real space the displacements are turned through $\frac{1}{2}\pi$ and scaled by $\hbar/eB$. Collisions are taken into account by supposing each electron, on suffering a catastrophic collision, to stop dead at that point, and L_i is the ultimate vector position of the centroid after all have collided. Consider the first half-cycle until the moment when Δ_1 returns to zero, during which time all but a fraction $\exp(-\pi\gamma N/\omega_c\tau)$ suffer collisions. In an interval dt a fraction $\exp(-t/\tau)\,dt/\tau$ of the electrons are stopped with displacements $\Delta_1 = (t-\omega_c t^2/\pi\gamma N)\,\omega_c K_1/\pi\gamma N$, $\Delta_2 = \omega_c K_2 t/\pi\gamma N$, and the centroid of the whole group is readily calculated to lie at $(\Delta_1^{(1)}, \Delta_2^{(1)})$, where

$$\Delta_1^{(1)} = (\coth z - z^{-1})\,K_1/2z \tag{23}$$

and

$$\Delta_2^{(1)} = \tfrac{1}{2}K_2 - \tfrac{1}{2}K_2(\coth z - z^{-1}), \tag{24}$$

z being written for $\pi\gamma N/2\omega_c\tau$. In successive half cycles the centroids of scattered electrons are given by the same expressions, except for sign reversal in $\Delta_1^{(1)}$ and in the second term of $\Delta_2^{(1)}$. The fraction scattered in the nth half cycle is $e^{-2(n-1)z}(1-e^{-2z})$, and the ultimate position of the centroid of all particles is found by summing geometric series:

$$\Delta_1 = (1-e^{-2z})\,\Delta_1^{(1)}\sum_0^\infty (-1)^n e^{-2nz} = (1-z^{-1}\tanh z)\,K_1/2z$$

and

$$\Delta_2 = (\tfrac{1}{2}K_2/z)\tanh z.$$

Translated into real space by scaling and rotating, the mean value of L_i is

$$\bar{L}_1 = \hbar K_1(1-z^{-1}\tanh z)/2eBz \tag{25}$$

and

$$\bar{L}_2 = (\hbar K_2/2eBz)\tanh z. \tag{26}$$

In the present applications we imagine k space sliced, normal to $\boldsymbol{B}$, into sections of thickness δ, and a given orbit in such a section contributes to the conductivity an amount that follows directly from (22) by writing $\oint L_i\,dS_j$ as $2\bar{L}_i K_j\delta$. The quantity that we have designated σ_1 elsewhere, the conductivity along the easy direction, is σ_{11}, and therefore

$$\sigma_1 = eK_1^2\delta(1-z^{-1}\tanh z)/4\pi^3 Bz = \omega_c^2\tau^2 ek_\parallel^2\delta(z-\tanh z)/\pi^5\gamma^2 B, \tag{27}$$

since $k_\parallel = K_1/N$. Further

$$\sigma_{21} = (eK_1K_2\delta/4\pi^3 Bz)\tanh z. \tag{28}$$

It will be noted that since $K_1K_2\delta/4\pi^3$ is the number of electrons per unit volume, n_0, contained in the orbit, then at large values of $\omega_c\tau$, as z tends to zero, σ_{21} becomes $n_0 e/B$, the standard high field limit for the Hall conductivity. Hence $1-z^{-1}\tanh z$ is the fractional deficit of the Hall conductivity from this limit, i.e. $\Delta\sigma_{12}/\sigma_H$, and is closely related to σ_1 as given by (27):

$$\Delta\sigma_{21}/\sigma_1 = K_2 z/K_1 = \pi\gamma^2 A_e/2\omega_c\tau k_\parallel^2. \tag{29}$$

For highly extended or open orbits, when N and z become large, the fractional Hall deficit increases to unity (open orbits have no Hall conductivity) and σ_1 tends to $Nek_\parallel^2\delta\omega_c\tau/2\pi^4\gamma B$, independent of B (since $\omega_c \propto B$) and proportional to the orbit length.

Finally the results may be translated into the units used elsewhere in this paper, with the distance between neck centres taken as the unit of k; then (27) takes the form:

$$\sigma_1 = 2\omega_c^2\tau^2 k_\parallel^2\delta\sigma_H(z-\tanh z)/\pi^2\gamma^2, \tag{30}$$

while σ_{21} is derived from it by use of (29), which is unaltered.

Enumeration of orbits

(a) *Periodic extended orbits*

When (θ, ϕ) lies outside the shaded areas of figure 1, all orbits are closed and electron-like, but just outside some are very long and dominate the conductivity. Two types of highly extended orbit have to be considered. First those lying near the high symmetry planes which we shall call periodic extended orbits, since they are finite versions of the periodic open orbits found exactly on the high symmetry planes, such as that shown in figure 9; and secondly those lying near the boundary of the shaded areas which we shall call aperiodic extended orbits, since inside the boundary the open orbits are aperiodic in character. The former are readily understood from figure 4(*a*) which refers to an orientation near the (100) plane. Exactly on the plane, where $\phi = 0$, the contour of the $\boldsymbol{B}$ plane is strictly vertical and can intersect an unlimited number of P lines to generate a periodic open orbit. In this case there are two different open orbits, formed by alternate intersection of the necks a and d, and of the necks b and c. When ϕ is non-zero but small it is good enough to take $P_a = P_d$ and $P_b = P_c$, as in the (100) plane itself, and the lengths of the extended orbits are clearly $2P_a/\phi$ and $2P_b/\phi$ units; all other orbits present are short, no more than one or two units. Let us overlook for the moment the presence of highly extended orbits of two different lengths at each orientation of $\boldsymbol{B}$, and suppose that all have the same length, $2P\phi^{-1}$, or $2p\phi^{-1}\operatorname{cosec}\theta$. This fixes the value of K_1 to be inserted in (27) and (28). The number of extended orbits is found by imagining a single replica of the Fermi surface sectioned into slices of thickness δ. Since there are 4 necks, each of thickness $2p$ measured normal to the slices, the necks are cut $8p/\delta$ times. Now each extended orbit is of length $2p\phi^{-1}\operatorname{cosec}\theta$ and involves $2p\phi^{-1}\operatorname{cosec}\theta$ necks, from from which it follows that there are $4\phi\delta^{-1}\sin\theta$ separate orbits. Multiplying (30) by this factor, and putting $k_\parallel = \gamma = 1$ and $z = (\pi p/\omega_c\tau\phi)\operatorname{cosec}\theta$, we have that

$$\sigma_1 = 8\omega_c\tau\sigma_H p(1 - z^{-1}\tanh z)/\pi.$$

This can be cast in a convenient standard form:

$$\sigma_1 = \sigma_1(0)\left[1 - \frac{\epsilon}{\alpha}\tanh\left(\frac{\alpha}{\epsilon}\right)\right]. \tag{31}$$

in which $\sigma_1(0) = 8\omega_c\tau\sigma_H p/\pi$ and is the conductivity along the open orbit direction when $\boldsymbol{B}$ lies in the (100) plane; $\epsilon = \phi\sin\theta$ and is the angular distance from the (100) plane measured along the great circle; $\alpha = \pi p/(\omega_c\tau)$. Hence, by use of (29), the Hall deficit may be derived:

$$\Delta\sigma_{21} = 4pA_e\sigma_H\left[1 - \frac{\epsilon}{\alpha}\tanh\left(\frac{\alpha}{\epsilon}\right)\right], \tag{32}$$

where A_e is given by figure 10.

In deriving (31) for $\boldsymbol{B}$ lying in the (100) plane we ignored the distinction between the two pairs of necks, and strictly (31) should be the sum of two similar terms, with $\sigma_1(0)$ equal to $4\omega_c\tau\sigma_H p_a/\pi$ or $4\omega_c\tau\sigma_H p_b/\pi$ and $\alpha = \pi p_{a,b}/(\omega_c\tau)$. This adds very considerably to the labour of computing average conductivities, since the relative weight of each term depends not only on θ but, through $\omega_c\tau$, on B. The extended orbits in question, however, contribute only about 12 % to $\overline{\sigma}_{xx}$ and it was therefore decided to simplify the process by taking a suitable average. To give the correct value of $\sigma_1(0)$ and hence get the best match for those most important crystallites containing highly extended orbits, p in $\sigma_1(0)$ was taken as $\frac{1}{2}(p_a + p_b)$; and since the Ziman approximation,

$\overline{\sigma}_{xx} = \langle \sigma_{xx} \rangle$, is not too bad it was decided to choose α so that $\int \sigma_1 \mathrm{d}\phi$ was correctly matched. Now

$$\int_0^\infty \sigma_1 \mathrm{d}\epsilon = \alpha_1(0) \int_0^\infty (z - \tanh z)\, \mathrm{d}z/z^3 = 0.852 \alpha \sigma_1(0), \tag{33}$$

and the match was effected by taking $\alpha\sigma_1(0)$ as the mean of the two values; in other words, p was taken as $(p_a^2 + p_b^2)/(p_a + p_b)$ in calculating α.

This problem does not arise with the other periodic extended orbits, for which the form (31) applies directly, though the details of $\sigma_1(0)$ and α are different. It is helpful to imagine the (100) plane periodic open orbits to be generated by impaling the periodically extended Fermi surface on a $\boldsymbol{B}$ arrow running through two nearest neighbour necks. A plane containing this arrow then generates the open orbit sections. For the (110) plane the arrow must run through next nearest neighbouring necks, while for the (111) plane it runs through opposite necks. In figure 1 the range of θ between A and B represents the angle through which the surface can be turned on the (100) arrow without generating hole orbits; these of course lie within the shaded regions round [100] and [110] and are dealt with separately. On the (110) arrow there are two relevant ranges of θ, represented by CD and EF, while on the (111) arrow it is GH that counts. It should be noted that when counting orbits in the basic triangle of the diagram, the periodic extended orbits must be taken as lying on one side only of the boundary lines AB, CD and EF, but on both sides of the internal line GH.

For the (110)-orbits we have $\phi = \frac{1}{4}\pi$ and θ is measured from [100]. Thus CD is the range of θ between 8.82° and 48.56°, while EF runs from 60.90° to 73.25° along the same great circles. Now $k_\parallel = \sqrt{2}$ and the main spine of the extended orbit involves only necks b and d; if necks a and c play a part, it is to increase the sinuosity. The counting of orbits proceeds as before, but the number is halved because only half the necks are involved, and multiplied by $\sqrt{2}$ because the longer $k_\parallel$ means that fewer necks are needed for an orbit of given length. Hence z is changed to $\pi\gamma p/\sqrt{2}\omega_c\tau\epsilon$, and (31) applies with the assignments as follows:

$$\sigma_1(0) = 8\omega_c\tau\sigma_H p/\pi\gamma \quad \text{and} \quad \alpha = \pi\gamma p/\sqrt{2}\omega_c\tau. \tag{34}$$

Also

$$\Delta\sigma_{21} = 2\gamma p A_e \sigma_H \left[1 - \frac{\epsilon}{\alpha} \tanh\left(\frac{\alpha}{\epsilon}\right)\right]. \tag{35}$$

The value of γ needs discussion. At the boundary of the open orbit zone round [100], $\gamma = 2$ according to (14). As θ is increased, however, and P becomes smaller, the average number of necks cut in each row decreases; moreover, some of the cuttings do not increase γ but belong to isolated two-unit orbits of no account. Since the matter is of minor importance only, we merely state the result of analysis, that as θ goes from 8.8° to 14.3° γ falls linearly from 2 to 1.31 and then, between 14.3° and 20.8° falls with a different slope to unity, where it remains.

Next, the periodic extended orbits around the (111) plane for which $k_\parallel = \sqrt{3}$ and to the spine of which only one neck contributes. Compared with the (100) plane, the number of orbits is multiplied by $\frac{1}{4}\sqrt{3}$, so that

$$\sigma_1(0) = 6\omega_c\tau\sigma_H p/\pi\gamma \quad \text{and} \quad \alpha = \pi\gamma p/\sqrt{3}\omega_c\tau. \tag{36}$$

Also

$$\Delta\sigma_{21} = \gamma p A_e \sigma_H \left[1 - \frac{\epsilon}{\alpha} \tanh\left(\frac{\alpha}{\epsilon}\right)\right]. \tag{37}$$

Around the great circle from H to G is an arc of 19.65°; in the first 9.5° γ remains at unity, and then rises linearly to 2 at G.

Having cast σ_1 into a convenient standard form we may proceed to evaluate the contribution of periodic extended orbits to the averages P_{xx} and ΔP_{xy} occurring in (11) and (12). The normalized statistical weight of an element of solid angle $(\mathrm{d}\theta, \mathrm{d}\epsilon)$ is $12\,\mathrm{d}\theta\,\mathrm{d}\epsilon/\pi$ when the basic triangle of figure 1 defines the domain of integration; when $\omega_c\tau$ is large, so that only regions near the boundary contribute significantly, we have as the contribution of these regions

$$P_{xx} = \frac{12}{\pi}\int \mathrm{d}\theta \int_0^\infty \sigma_1 \mathrm{d}\epsilon/(\bar{\sigma}_{xx} + \lambda\sigma_1),$$

and

$$\Delta P_{xy} = \frac{12}{\pi}\int \mathrm{d}\theta \int_0^\infty \Delta\sigma_{21} \mathrm{d}\epsilon/(\bar{\sigma}_{xx} + \lambda\sigma_1).$$

Now define:

$$\sigma_r = 2\pi\sigma_1(0)/\omega_c\tau\sigma_H,$$

$$S = \lambda\omega_c\tau\sigma_H/2\pi\bar{\sigma}_{xx},$$

$$H = \tfrac{1}{4}A_c\gamma^2/k_\parallel^2,$$

$$y = S\sigma_r = \lambda\sigma_1(0)/\bar{\sigma}_{xx},$$

$$Y(y) = 1.174\int_0^\infty \mathrm{d}z/[z^2(y + (1 - z^{-1}\tanh z)^{-1})].$$

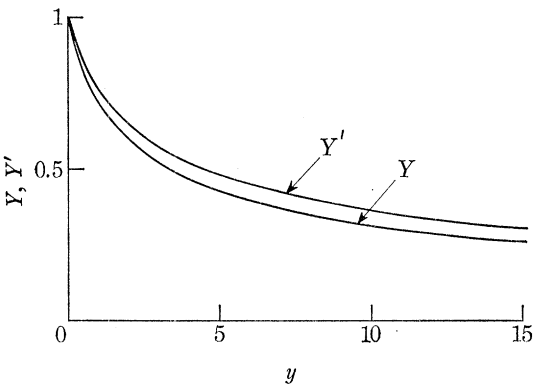

FIGURE 12. The functions $Y(y)$ and $Y'(y)$.

Then on substituting for σ_1 in the standard form (31) we have for the contributions of the periodic extended orbits

$$P_{xx} = \sigma_H I_A/\bar{\sigma}_{xx} \quad \text{and} \quad \Delta P_{xy} = 2\pi\sigma_H I_B/\omega_c\tau\bar{\sigma}_{xx}, \tag{38}$$

where $I_A = \int \beta p^2 Y \mathrm{d}\theta$, $I_B = \int H\beta p^2 Y \mathrm{d}\theta$, and β is a numerical factor equal to 26.03 for the (100) zone, 18.41 for the (110) zone and 22.54 for the (111) zone. The quantities p^2, σ_r and H are determined by the Fermi surface geometry alone, and vary with θ, while y in addition is determined by the sample and magnetic field strength through the multiplier S, which is independent of θ. The function $Y(y)$ is shown in figure 12.

(*b*) *Aperiodic extended orbits*

This disposes of the most important periodic extended orbits, but leaves a residual problem of some difficulty. In principle the impalement of two necks need not be limited to necks close enough to lie within a single Brillouin zone. Any two necks on the periodically extended Fermi surface may generate a zone on which periodic open orbits lie, flanked by highly extended orbits.

Measurements on single crystals (Klauder *et al.* 1966) show clearly how these zones extend, in the form of lines radiating from the symmetry points, into the central region of figure 1 where we have shown no open or highly extended orbits. Figure 13 is taken from their paper; the longest spikes belong to the zones of lowest rational indices. It would not be merely tedious to enumerate these zones systematically and take account of their associated regions of exceptional conductivity: it would be hard to ensure that one neither omitted some regions nor doubly counted some others.

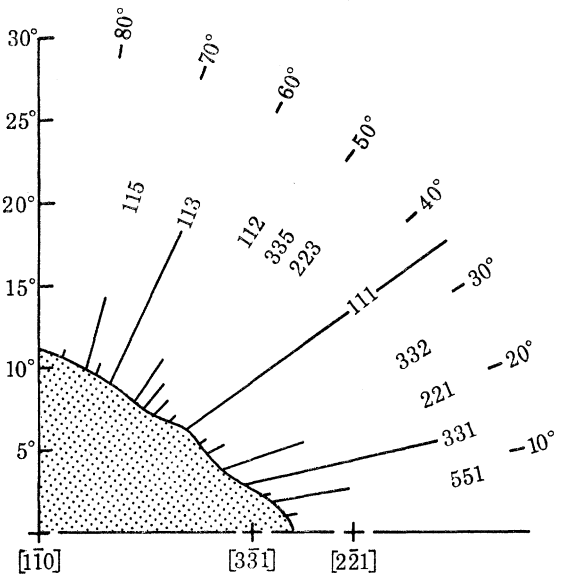

FIGURE 13. Higher order periodic open orbit zones around [110] (from Klauder *et al.* 1966, figure 9).

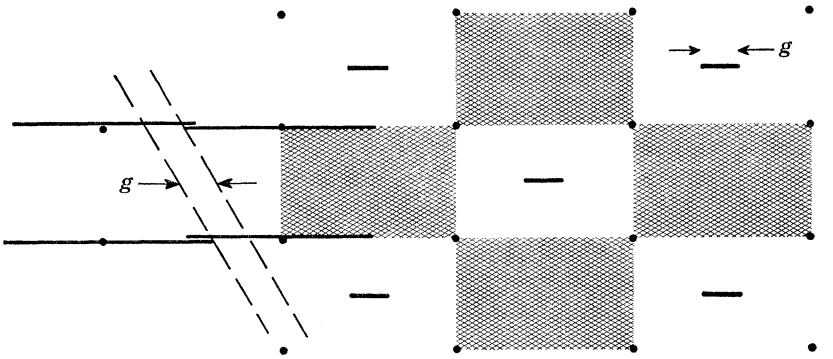

FIGURE 14. Replacement of P lines by targets.

The way we have chosen to circumvent this problem may seem contrived, but some measure of empirical justification is possible, based on Fickett's (1972) observation that the resistance of a very pure sample in a strong field is not greatly changed by raising the temperature to 15 K, even though this introduces a considerable amount of small angle phonon scattering and markedly alters the magnetoresistance of a single crystal (Pacher 1974). We shall therefore proceed on the assumption that small angle scattering is present and make use of the simplification permitted by statistical averaging.

Just outside the boundary of an open-orbit zone the condition for achieving a hole orbit, illustrated in figure 4(f), fails for a contour that runs through without cutting the P lines at

necks b and d; this is the only terminal pattern very close to the boundary where the highly extended orbits occur. It is now convenient to replace the P line pattern by a short 'target' in each alternate cell of the pattern, the length of the target, g, being just the gap,

$$k_1 + k_2 \tan\phi - (P_b + P_d)$$

according to (13), within which the contour must lie to cause the orbit to terminate. This is illustrated in figure 14. A contour running across this array of targets at an irrational angle will be dissected into a variety of lengths and only a very simple computation is needed to draw up a histogram of orbit lengths to be found in any given case. A few trials reveal the nature of the resulting problem. With targets of length 0.1 the mean orbit length is 20 units, but three choices of ϕ lying within $\frac{1}{2}°$ produced orbit lengths as given below, with percentage of their occurrence in brackets:

$\tan\phi = 0.5567$,	$\phi = 29.105°$:	122 (2.6 %)	113 (7.7 %)	9 (89.7 %)
0.5619,	29.332°:	32 (40.3 %)	23 (20.8 %)	9 (38.9 %)
0.5667,	29.540°:	37 (1 %)	23 (66 %)	14 (33 %).

The first row shows highly extended orbits separated by rather short orbits, and is to be understood as the consequence of $\tan\phi$ lying close to a rational fraction of low order, $\frac{5}{9}$, which would produce a spike in figure 13, though it would be hardly long enough to discover experimentally; exactly at this value of ϕ (29.055°) there would be open orbits, and in their vicinity would be found highly extended orbits like those in the top row. The second row shows what happens even closer to a rational direction of rather higher order, $\frac{9}{16}$, while the third is almost exactly on the direction of order $\frac{17}{30}$, yet neither gives a hint of open orbits close at hand. This is because there is no unobstructed path between targets in these rational directions. It is, indeed, easy to show that if $\tan\phi = n/m$, n and m being either both even or both odd (but otherwise having no common factor), a periodic open orbit exists only if the target length is less than $2k_1/n$ or $2k_1/m$, whichever is the smaller. In the present case the three values of ϕ lie between the spikes defined by $\frac{5}{9}$ (0.5555) and $\frac{11}{19}$ (0.5789), and one would have to move closer to the open orbit boundary to find any intermediate spikes. The picture that emerges is of a dense thicket of very short spikes extending from the open orbit boundary, and thinning out progressively at greater distances. It is in the densely packed region that small angle scattering may be invoked to circumvent the problem of taking averages over so wildly varying a function.

An open orbit in a direction of high rational order, depending as it does on the targets being very short, is acutely sensitive to small angle scattering, which causes the representative point of the electron in k space to leave the plane normal to $\boldsymbol{B}$, and thus to miss a neck it should have gone across, or vice versa. It is as if the contour determining which necks are cut were slightly jagged or, what comes to the same thing, as if the contour were straight but the targets were undergoing Brownian motion. Which targets are hit by the line is then subject to statistical variation, and in most directions of the contour it is so delicate a matter to thread through them in pursuit of a highly extended orbit that only a little Brownian motion is needed to randomise the behaviour almost perfectly. It is this model that we take to be empirically justified by the observation that the amount of phonon scattering matters little: almost any is enough to produce randomization.

The calculation of the conductivity now becomes straightforward for, as in elementary kinetic theory, the distribution of orbit lengths becomes exponential, with a mean length of $\bar{N}$ units,

$1/\bar{N}$ being $g/2k_1$, the probability that the contour hits a target as it crosses any one row. The number $\mathcal{N}(N)$ of orbits having length N is given by the expression

$$\mathcal{N}(N) = \frac{g^2 \sin\theta}{k_1^2 k_3 k_\parallel \delta} \mathrm{e}^{-gN/2k_1}, \tag{39}$$

the pre-exponential factor being determined by the requirement that the total length of the orbits in an area $4/\delta$ of the B plane is the overall length of the contour, $4\sin\theta/k_3\delta$. Combining this with (30) we have for the conductivity along the extended orbit direction

$$\sigma_1 = \sigma_1(0) \int_0^\infty \mu^2(z - \tanh z)\, \mathrm{e}^{-\mu z}\, \mathrm{d}z = \sigma_1(0) f(\mu), \tag{40}$$

in which $\mu = g\omega_c\tau/\pi\gamma k_1$ and $\sigma_1(0) = 4\omega_c\tau k_2 \sigma_H \sin\theta \sec\phi/\pi\gamma k_3$.

At the open orbit boundary, where $\theta = \theta_0, g = 0$; when $\omega_c\tau$ is large, as g increases on moving away from the boundary at constant ϕ, σ_1 decreases rapidly from $\sigma(0)$. It is then appropriate to write μ as $g'\omega_c\tau\epsilon/\pi\gamma k_1$, where $\epsilon = \theta - \theta_0$ and g' is the readily computed value of $\mathrm{d}g/\mathrm{d}\theta$ at the boundary. The contribution to P_{xx} of a sector between ϕ and $\phi + \mathrm{d}\phi$ may now be written down, for an element $\mathrm{d}\epsilon$ has weight $12\sin\theta_0\, \mathrm{d}\phi\, \mathrm{d}\epsilon/\pi$, and hence the contribution of each aperiodic extended orbit zone is cast in the same form as (38), with the following substitutions:

$$\left.\begin{aligned} &\beta p^2 \text{ is replaced by } 26.03\, k_1 k_2 \sin^2\theta_0 \sec\phi/k_3 g', \\ &Y \text{ is replaced by } Y'(y), \text{ defined as } 0.587 \int_0^\infty \mathrm{d}\mu/[y + 1/f(\mu)], \end{aligned}\right\} \tag{41}$$

and the integral is taken over ϕ within the range lying inside the basic triangle, i.e. $\frac{1}{4}\pi$ round [100] and $\frac{1}{2}\pi$ round [110]. The new function Y' is not very different from Y, as may be seen from figure 12, but the difference is enough to be taken seriously, even though the validity of the derivation is questionable. For the zones around [100] and [110], $k_1 k_2/k_3 = 1$; the zone around [111] needs special treatment to provide the result in the same form.

Around [111], as already discussed with reference to figure 6, an extended orbit is terminated if the contour passes between the P lines belonging to opposite points of a hexagon. The targets thus form a triangular net of spacing $2\sqrt{2}$, with g equal to $2(\sqrt{2} - P)$, and the behaviour is the same as for a rectangular net having $k_1 = \sqrt{2}$, $k_2 = \sqrt{6}$; successive layers of necks are $1/\sqrt{3}$ apart, so that $k_1 k_2/k_3 = 6$. The range of ϕ within the triangle is $\frac{1}{3}\pi$, but because of symmetry only half this need be taken and the resulting integral doubled, to give a contribution to P_{xx} of the standard form as in (41), but with the coefficient 26.03 replaced by 312.4. It might be thought that in consequence these orbits would contribute strongly, but the presence in g' of $\operatorname{cosec}\theta_0$ causes βp^2 to vary as $\sin^3\theta_0$, and the small values of θ_0 around [111] result in a relatively minor contribution from this source.

For the contribution of all these aperiodic extended orbits to ΔP_{xy}, A_e has been assigned the value for the central neck section when $\boldsymbol{B}$ lies along the relevant symmetry axis, as given in (21).

Open and hole orbits

Around the symmetry directions, when $\theta < \theta_0$, hole orbits and open orbits are present, the former, not being extended, contributing virtually nothing to σ_1 but having importance in $\Delta\sigma_{xy}$, while the latter contribute to both. Let us consider how the length of the P lines alters as we proceed, at constant ϕ, from θ_0 towards the symmetry point where θ vanishes. Around [100] there are 4 values of P, different at each corner of a square in figure 4, though all must converge to the

same value when $\theta = 0$. To a good approximation, since θ is small and p does not change rapidly, we may write each P, i.e. p cosec θ sec ϕ, in the form $(p_0/\theta + p')$ sec ϕ, in which only the second term, representing $\mathrm{d}p/\mathrm{d}\theta$, is different for each corner, and this is independent of θ. Consequently, as the P lines increase in length with decrease of θ, the differences between them stay constant, and therefore the pattern of crosses at the sides of the hole orbit region remains roughly the same. Since this pattern determines the sinuosity of the open orbits, we take γ to be independent of θ, fixed only by ϕ according to (14). Since the mean value of p' is zero, the mean length of the P lines $\propto 1/\theta$ and the average number of crosses per line is $\gamma\theta_0/\theta$, of which γ are taken up by open orbits and $\gamma(\theta_0/\theta - 1)$ by hole orbits. The contribution of open orbits to σ_1 varies with θ only insofar as the spacing of contours varies as $1/\theta$, and hence the total number of electrons associated with open orbits is proportional to θ. The hole orbits contribute to $\Delta\sigma_{xy}$, through $\gamma\theta_0/\theta$, a constant term and, through $-\gamma$, a negative term proportional to θ; these two together vanish at θ_0, but there is still a contribution to the Hall deficit from electrons moving on open orbits. All that is needed is to determine σ_1 and σ_{xy} at the symmetry point and at θ_0, and to interpolate linearly between them. At θ_0 we already have that $\sigma_1 = \sigma_1(0)$ and $\sigma_{xy} = H\sigma_1(0)$, while at the symmetry points the geometry of the Fermi surface determines the proportion of electrons in hole orbits, being simply the proportion in the slices defined by the necks.

At [100], if the overall thickness of the neck zones, $4p$ in this case, is h, a volume hA_e containing electrons is converted to a volume hA_h of holes, leaving $2 - hA_e$ electrons. The electron count is therefore reduced from 2 to $2 - h(A_e + A_h)$, i.e. $2 - 2h$, and the Hall deficit is simply $h\sigma_H$, or $0.432\sigma_H$, according to (16) and (17). A similar argument gives h as $2p$ and the deficit as $\sqrt{2}h\sigma_H$, or $0.416\sigma_H$, for [110]. For [111] it must be remembered that one hexagonal hole orbit is gained for every two triangular electron orbits lost, and the deficit is $\sqrt{3}h\sigma_H$, where h is now $4p$ since there are two neck zones; the resulting deficit is $0.939\sigma_H$. In summary, if the Hall deficit is written as $f_0\sigma_H$, $f_0 = 0.432$, 0.416 and 0.939 for the three principal directions.

The contribution of open orbits to P_{xx} may be written down immediately by noting that an element $(\mathrm{d}\phi, \mathrm{d}\theta)$ has weight $12\theta\,\mathrm{d}\theta\,\mathrm{d}\phi/\pi$, if $\sin\theta$ is replaced by θ as in the rest of this calculation, and that the value of σ_1 is $\sigma_1(0)\,\theta/\theta_0$. The sector $\mathrm{d}\phi$ thus contributes $\mathrm{d}P_{xx}$, where

$$\mathrm{d}P_{xx} = (12\,\mathrm{d}\phi/\pi\lambda)\int_0^{\theta_0}\theta^2\,\mathrm{d}\theta/(\theta + \theta_0/y) = (12\theta_0^2\,\mathrm{d}\phi/\pi\lambda)\,[\tfrac{1}{2} - 1/y + \ln(1+y)/y^2], \tag{42}$$

y having the same meaning, $\lambda\sigma_1(0)/\overline{\sigma}_{xx}$, as before. Once $\overline{\sigma}_{xx}$ has been chosen, numerical integration over ϕ round each symmetry point is straightforward, and produces contributions to P_{xx} in the form

$$P_{xx} = (1/\lambda S^2)\int CyZ_2(y)\,\mathrm{d}\phi, \tag{43}$$

in which $Z_2(y) = \frac{1}{2}y - 1 + \ln(1+y)/y$, and $C = 12\theta_0^2/\pi\sigma_r^2$. For ΔP_{xy}, linear interpolation between 0 and θ_0 gives for $\Delta\sigma_{xy}/\sigma_H$ the expression $f_0 - (f_0 - H\sigma_1(0))\,\theta/\theta_0$, and integration over θ, similar to that for P_{xx}, gives for the contribution of a sector $\mathrm{d}\phi$:

$$\mathrm{d}(\Delta P_{xy}) = (12\theta_0^2\sigma_H\,\mathrm{d}\phi/\pi\overline{\sigma}_{xx})\,[f_0(1/y - \ln(1+y)/y^2) - (f_0 - H\sigma_r)\,(1/2y - 1/y^2 + \ln(1+y)/y^3)], \tag{44}$$

which once more depends on the choice of $\overline{\sigma}_{xx}$. The combined contributions of open and hole orbits to ΔP_{xy} may then be written

$$\Delta P_{xy} = (\sigma_H/S^2\overline{\sigma}_{xx})\int[DZ_1(y) + EZ_2(y)]\,\mathrm{d}\phi, \tag{45}$$

in which $D = 12\theta_0^2 f_0/\pi\sigma_r^2$ and $E = 12\theta_0^2(H\sigma_r - f_0)/\pi\sigma_r^2$.

Summary and basis of computation

The variation of the relevant parameters round the boundary in figure 1 is shown in figure 15, and this is the information from which P_{xx} and ΔP_{xy} can be computed by use of (38), (43) and (45), together with the modified interpretation, where appropriate, of βp^2 and Y given in (41). To compute $\overline{\sigma}_{ij}$ the experimental conditions are summed up in the value of S, and thus the

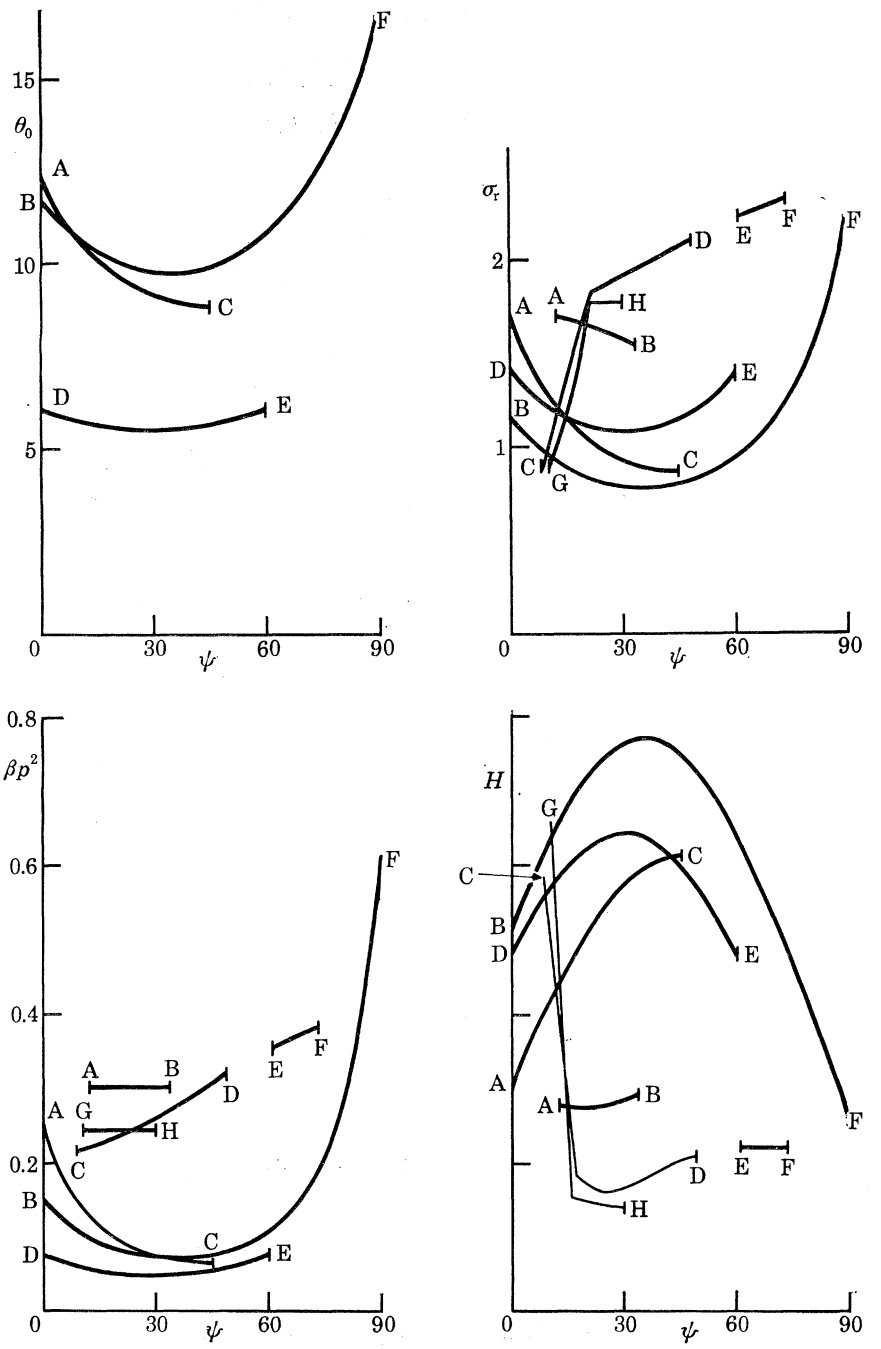

Figure 15. Graphical summary of geometrical data used in computations; ψ denotes either θ or ϕ as appropriate, and the letters relate to figure 1.

integrals occurring in P_{xx} and ΔP_{xy} are needed as functions of S. The computation presents no difficulties and the results are conveniently displayed as empirical functions that fit the computed values well enough. Thus we write

$$P_{xx} = \sigma_{\mathrm{H}} I_{\mathrm{A}}/\overline{\sigma}_{xx} + I_{\mathrm{c}}/\lambda S^2 \tag{46}$$

and

$$\Delta P_{xy} = \sigma_{\mathrm{H}}^2 \lambda I_{\mathrm{B}}/S\overline{\sigma}_{xx}^2 + \sigma_{\mathrm{H}} I_{\mathrm{D}}/S^2\overline{\sigma}_{xx}, \tag{47}$$

in which

$$I_{\mathrm{A}} = \int \beta p^2 Y \,\mathrm{d}\psi \approx 10^{-2}[62 - 39.9 \lg S - (\lg S - 0.55)^2 + 9.3(\lg S - 0.18)^3]$$

$$I_{\mathrm{B}} = \int H\beta p^2 Y \,\mathrm{d}\psi \approx 10^{-2}[22.5 - 13.8 \lg S - 0.6(\lg S - 0.55)^2 + 3.3(\lg S - 0.24)^3]$$

$$I_{\mathrm{C}} = \int CyZ_2 \,\mathrm{d}\phi \approx 10^{-2} S^2[7.35 + 9.69 \lg S - 3.52(\lg S - 0.17)^3]$$

$$I_{\mathrm{D}} = \int (DZ_1 + EZ_2)\,\mathrm{d}\phi \approx 10^{-2} S[5.7 + 8.8 \lg S - 2.4(\lg S - 0.3)^3].$$

In I_{A} and I_{B}, $\mathrm{d}\psi$ comprises $\mathrm{d}\theta$ for integration round the periodic orbit boundaries and $\mathrm{d}\phi$ for integration round the aperiodic orbit boundaries.

To relate the parameters to the measured characteristics of copper, expressions are needed for σ_{H} and $\omega_{\mathrm{c}}\tau$. By definition σ_{H} takes the free electron value ne/B, i.e. $1.377/B \times 10^{10}\,\Omega^{-1}\,\mathrm{m}^{-1}$, while for a quasi-free electron metal $\omega_{\mathrm{c}}\tau$ is just $\sigma/\sigma_{\mathrm{H}}$ which may be written as $4.66 \times 10^{-3} BR$, in which R is the resistance ratio, ρ_{273}/ρ_0. The values of $\omega_{\mathrm{c}}\tau$ relevant to the calculation are, however, not the free electron values but those for electrons moving in orbits that pass near or through the necks, and both ω_{c} and τ may be altered by this. Considerable uncertainty must therefore attach to the values used, since experimental evidence is scanty, and in any case τ is likely to differ for different samples of the same conductivity, if the scattering centres are different in kind. Fortunately, however, the calculations are not very sensitive to the choice of $\omega_{\mathrm{c}}\tau$; in particular, if Kohler's rule is obeyed and the resistivity is strictly proportional to B, there is, as will be discussed later, no dependence of resistivity on τ. This was remarked on by Fickett (1972) whose experiments largely confirm expectation. We shall therefore introduce a coefficient a, assumed in the first place to be the same for all orbits, though this will turn out to be too simplistic a model; nevertheless we start by writing

$$\omega_{\mathrm{c}}\tau = 4.66 \times 10^{-3} BR/a, \tag{48}$$

and calculate the magnetoresistance behaviour for a range of choices of a. A little information concerning the value to be chosen for a may be gleaned from the longitudinal magnetoresistance, and we shall discuss this briefly in the next section before turning to the more interesting transverse effect. Before doing so, however, let us note the form of a typical Kohler plot according to the present theory. If $\overline{\rho}_{zz}$ has saturated at $2\rho_0$, and we put $a = 1$, the logarithmic plot of figure 16 results. The broken curve at the left indicates that the theory is inapplicable when $\omega_{\mathrm{c}}\tau$ is small, for the assumption that $\overline{\sigma}_{xx}$ is dominated by highly extended orbits is untenable. The full curve is the result of joining the upper portions of the theoretical curve to the experimental curve at relatively low field strengths, and without straining produces a very nearly linear variation of $\overline{\rho}_{xx}$ with B until $\overline{\rho}_{xx}/\rho$ is something like 150. Ultimately, of course, saturation sets in at such high values of B that only the open orbits are left to contribute to $\overline{\sigma}_{xx}$; but this is well beyond the scope of any experiments performed hitherto.

The limitations of the theory at small $\omega_c\tau$ are also revealed by the curves in figure 17 of $\bar{\sigma}_{xx}/\sigma_H$ and $\bar{\sigma}_{xy}/\sigma_H$ which, combined as in (1), yield $\bar{\rho}_{xx}$. At the left, where $\omega_c\tau$ is small, $\bar{\sigma}_{xy}$ falls away from the free electron value as more of the extended orbits become longer than a free path and fail to make their full contribution to the Hall conductivity. Clearly the assumption of the theory, that only a small fraction of the electron count is lost thereby, becomes dubious as BR falls below 5000. It may also be noted in this diagram how $\bar{\sigma}_{xx}/\sigma_H$ rises when $\omega_c\tau$ is large, since $\bar{\sigma}_{xx}$ tends to a constant limit set by the open orbits while σ_H falls as $1/B$. The crossing of the two curves when $BR \approx 4\times 10^4$ will acquire significance in the discussion of experimental results.

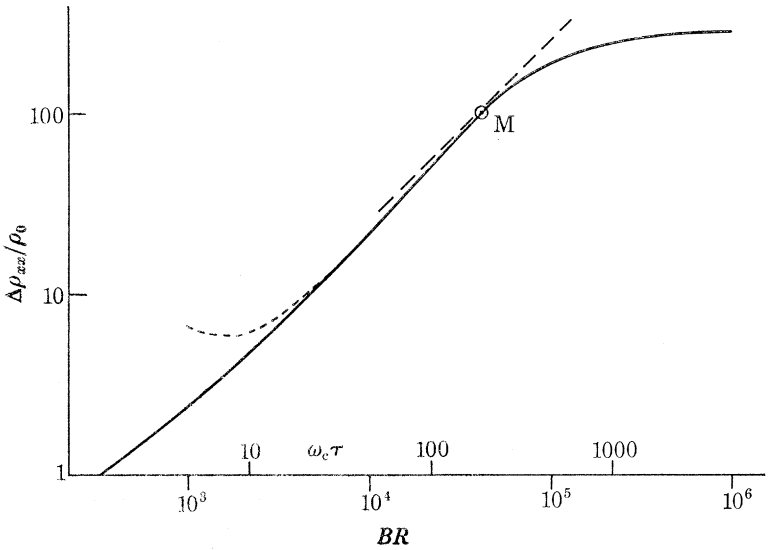

FIGURE 16. Typical logarithmic Kohler plot of computed transverse resistivity. No allowance is made for small angle scattering. At M the tangent has unit slope. The broken curve on the left shows the failure of the approximations at small values of $\omega_c\tau$.

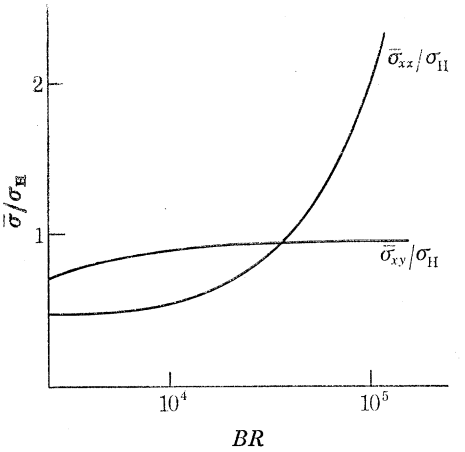

FIGURE 17. Variation of $\bar{\sigma}_{xx}$ and $\bar{\sigma}_{xy}$ for the same assumptions as for figure 16.

LONGITUDINAL MAGNETORESISTANCE

The saturation of the longitudinal resistivity at a relatively low value, as we have just assumed, is an experimental result, with $\bar{\rho}_{zz}(B)/\rho(0)$ rising to something between two and four times the zero field value, depending on the samples. The effective medium theory can be readily modified

to apply here, and the details need not be presented, only the final expression determining the resistivity $\bar{\rho}_{zz}$ of the polycrystalline sample:

$$\langle (1+\lambda_1)/(1+\lambda_1\rho_{zz}/\bar{\rho}_{zz})\rangle = 1,$$

where $\lambda_1 = 2\lambda/(1-\lambda)$ and is therefore fairly small in the cases of interest, becoming smaller as B increases. Since ρ_{zz} does not range nearly so widely σ_{xx}, the equivalent form of Ziman's conjecture is more applicable to this case, and we may take $\bar{\rho}_{zz}$ to be given by $\langle \rho_{zz}\rangle$, as if the current density were uniform.

The geometrical analysis needed to estimate the saturation value of ρ_{zz} for a given direction of $\boldsymbol{B}$ is considerably more tedious than for the transverse conductivity components, and since we need only fairly rough estimates a crude simplification will be adopted. The real Fermi surface is replaced by a sphere, on which are marked necks subtending the same solid angle as on the real surface. Any electron lying within a neck zone is assumed to contribute nothing to σ_{zz} (Pippard 1964), while those outside the neck zones are assumed unaffected by B. Values of ρ_{zz} computed in this way vary in a quite complicated fashion as $\boldsymbol{B}$ changes direction, according as different neck zones overlap or not. The lowest magnetoresistance occurs at [111], where the saturation value is 1.16 times the zero field value, and the highest at $\theta = 20°$, $\phi = 27°$ where the ratio is 2.8. The mean value of the ratio is about 1.7.

This is to be compared with the value of 2.0 determined by de Launay *et al.* (1959) on a sample of resistance ratio 606 prepared by casting *in vacuo*, and with values ranging between 2.6 and 4 (Martin *et al.* 1977) on samples annealed in oxygen at a low pressure and having resistance ratios 10 times greater or more. A natural interpretation is in terms of small angle scattering which is known to enhance the longitudinal magnetoresistance (Strom-Olsen 1967). Unfortunately one cannot proceed unequivocally from this to the effect of small angle scattering on open and extended orbits, since the dependence of each on the angular distribution of the scattered electrons is very different; nevertheless certain limits may be set. The enhancement of longitudinal magnetoresistance arises from the fact that scattering into a neck zone is as good as isotropic scattering when B is large, but not when B is small. Thus uniform scattering into a cone of, say, 20° half angle may be highly efficacious at high fields in those orientations for which there are plenty of neck zones, but in zero field several scattering processes may be needed to randomize the motion. The effective value of τ is thus reduced by a substantial factor as B increases, and the resistance reflects this behaviour. Similarly a scattering angle of 20° is easily enough to take an electron off an open orbit, and every scattering process will be effective. The enhancement of magnetoresistance can in this case be taken as a fair measure of the reduction factor a in (48). It is possible, however, that the scattering pattern has a stronger forward lobe than in this idealized model, and such a lobe may well be effective for open orbits and less effective for longitudinal magnetoresistance. Probably, then, we should take a as not less than the magnetoresistance enhancement, but we have no means of estimating how much larger it might be. In saying this, no account has been taken of ω_c for neck orbits, but this is unlikely to differ from the free electron value by as much as the uncertainty in τ.

The conclusion, then, is that in the sample used by de Launay *et al.* (1959) scattering was probably rather close to isotropic, and a may be taken as unity or a little more, while in the samples of Martin *et al.* (1977) a is at least 2 and might be considerably more. Fickett (1972) does not record any measurement of the longitudinal effect, but his sample preparation was similar to that of Martin *et al.*, and the higher figures for a seem appropriate.

PHILOSOPHICAL TRANSACTIONS OF THE ROYAL SOCIETY A MATHEMATICAL, PHYSICAL & ENGINEERING SCIENCES

As already hinted, the foregoing analysis neglects an important point, which is that small angle scattering need not affect σ_{12} nearly as strongly as σ_1. The Hall effect arises from the lateral displacement of an electron, even in a highly extended orbit, as a consequence of the non-vanishing width; thus an electron starting out on one long side of its orbit has a mean position, taken over many revolutions, lying on the spine. Now if the electron, instead of continuing to move in the extended orbit, is scattered through a small angle and then proceeds, as is most probable, to move on a small electron orbit, its mean position is laterally displaced by much the same amount. In this the behaviour differs from isotropic scattering, following which the electron is equally likely to move in any direction so that the mean position subsequently is just the point at which scattering occurred, with no lateral displacement. In a sample, therefore, in which the free path, as determined by the zero-field resistivity, is long, but where there is much small angle scattering, it is proper to assign a large value to a in calculating $\bar{\sigma}_x$, but a value near unity in calculating $\bar{\sigma}_{xy}$. We shall start, however, by ignoring this consideration, to see how well experiment and theory agree without the help of these rather imprecise speculations.

It may be significant that Fickett found Kohler's rule to apply rather closely to measurements made on differently prepared samples with widely differing values of R, but since the theoretical predictions are rather insensitive to the value of a it would be unwise to read too much into this result. By the same token any substantial discrepancies between theory and experiment cannot be attributed to incorrect choice of a in the computations. It is worth noting that this insensitivity of the theory is not accidental, but follows from Kohler's rule, itself an essentially dimensional consequence of certain restrictions applied to the scattering processes. For the rule to be obeyed it is only necessary that the Fermi surface geometry be constant and that variations of relaxation time over the surface follow a fixed law, so that the difference between one sample and another is characterized by the value of τ at any one point on the Fermi surface, and the value of B determines $\omega_c\tau$ for every orbit. Under these conditions the only dimensionless parameters that can be formed are $\bar{\rho}_{xx}(B)/\rho(0)$ and $\omega_c\tau$, and BR is a convenient measure of $\omega_c\tau$. From this Kohler's rule follows:

$$\bar{\rho}_{xx}(B)/\rho(0) = f(BR). \tag{49}$$

Now if we suppose that every orbit contributing to $\bar{\rho}_{xx}(B)$ has its value of τ diminished by the same factor a, and if the same a governs the enhancement of the longitudinal magnetoresistance, then every process that matters is such that the value of $\rho(0)$ to be inserted in (49) is not the measured value, $\rho(0)$, but $a\rho(0)$, and similarly R should be replaced by R/a. The modified form of (49) is therefore as follows:

$$\bar{\rho}_{xx}(B)/\rho(0) = af(BR/a). \tag{50}$$

On a logarithmic Kohler plot curves for different values of a are identical in shape, but shifted bodily along a 45° line; in particular, when $\bar{\rho}_{xx}(B) \propto B$, the shift leaves the curve unchanged, so that $\bar{\rho}_{xx}(B)/\rho(0)$ is independent of a. If, however, the longitudinal magnetoresistance is not governed by a, the form of the functional relationship changes; nevertheless, computation shows only a rather slight sensitivity of the shape in this case.

Comparison with experiment

If the resistance is strictly proportional to B, and the assumptions underlying (50) hold, $\bar{\rho}_{xx}(B)$ is determined by B alone, R and a being irrelevant. It is convenient then to compare theory and experiment by means of the transverse resistivity itself, rather than by a Kohler plot.

(a) *The Ziman limit*

If $\overline{\sigma}_{zz}$ is allowed to increase without limit, λ and S go to zero and Ziman's conjecture is valid. The limiting values of the integrals in (46) and (47) are as follows:

$$I_A \simeq 0.92, \quad I_B \simeq 0.32, \quad I_C \simeq 0.14S^3, \quad I_D \simeq 0.10S^2.$$

Hence
$$P_{xx} \simeq (0.92 + 0.14\omega_c\tau/2\pi)\,\sigma_H/\overline{\sigma}_{xx},$$
and
$$\Delta P_{xy} \simeq (0.32 \times 2\pi/\omega_c\tau + 0.10)\,\sigma_H/\overline{\sigma}_{xx}. \qquad (51)$$

Then, according to (11) and (12),

$$\overline{\sigma}_{xx}/\sigma_H \simeq 0.46 + 0.07\omega_c\tau/2\pi,$$
and
$$\overline{\sigma}_{xy}/\sigma_H \simeq 0.90 - 0.32 \times 2\pi/\omega_c\tau. \qquad (52)$$

In the experiments of de Launay *et al.* (1959) BR took values up to about 6000 where, according to (48), $\omega_c\tau = 28$ if $a = 1$. Then $\overline{\sigma}_{xx}/\sigma_H = 0.77$ and $\overline{\sigma}_{xy}/\sigma_H = 0.83$. Hence, from (1),

$$\overline{\rho}_{xx}(B) = 0.60/\sigma_H = 4.4 \times 10^{-11} B\,\Omega\mathrm{m};$$

this is to be compared with the measured value of 3.6×10^{-10} in a field of 10T, a discrepancy of only about 20 %. However, when the measured value of $\overline{\sigma}_{zz}$ is used to calculate λ, S is found to take the value 0.82, so that y typically lies around unity, and $Y(y)$ is nearer to 0.7 than to 1 as implied by Ziman's conjecture. Consequently $\overline{\sigma}_{xx}$ and hence $\overline{\rho}_{xx}$ are overestimated by this procedure. A further indication of the limitations of Ziman's conjecture is provided by the saturation value of $\overline{\rho}_{xx}(B)$; as $\omega_c\tau \to \infty$, $\overline{\sigma}_{xx}/\sigma_H \to 0.011\omega_c\tau$, compared with which $\overline{\sigma}_{xy}/\sigma_H$ is negligible. Then $\overline{\rho}_{xx}(B)/\rho(0)$, which is equal to $\omega_c\tau\sigma_H\overline{\rho}_{xx}(B)$, tends to the value 90, which is less than values that have been observed while $\overline{\rho}_{xx}(B)$ is still rising almost linearly. As is already clear from figure 16, the effective medium approximation gives considerable help here by raising the theoretical saturation value substantially.

(b) *Effective medium approximation*

The theoretical results of figure 16 are presented once more in figure 18, but now as values of $\overline{\rho}_{xx}(B)$ when $B = 10$T; the lower values of BR, where the theory has been found wanting, are not included. Also shown is the very slight effect of changing a from 1 to 1.25 while keeping the same longitudinal magnetoresistance. Scaling of the longitudinal ratio $\overline{\rho}_{zz}(B)/\rho(0)$ and a by the same factor (2 as shown) simply translates the curve horizontally. If the results of Martin *et al.* (1977) are typical, one might expect the measured curve for a series of samples of different R to follow curve I when R is small, shifting towards III, or beyond, when R is large, perhaps yielding something like IV. This does, however, suppose that the same value of a applies to $\overline{\sigma}_{xx}$ and $\overline{\sigma}_{xy}$; it is more likely that $\overline{\sigma}_{xy}$ should be allowed to remain at about $0.95\sigma_H$, while the enhanced small angle scattering when R is large raises a and thus also prevents $\overline{\sigma}_{xx}$ from rising. Instead of a falling away of $\overline{\rho}_{xx}$ at high values of R, a levelling off is to be expected at some point beyond the value achieved by de Launay *et al.*, and probably therefore after the slight minimum shown in I and and IV. The results presented by Fickett are reproduced as V, and the value obtained by de Launay *et al.* fits very well on this, as indicated by the cross. It is here that theory and experiment are as well in agreement as could be hoped, but purer samples reveal a sizeable discrepancy.

Not only are the measured values of $\overline{\rho}_{xx}(B)$ markedly lower than predicted, but there is no sign of a minimum, let alone a hump, as in the theoretical curves, and this is not a trivial matter. For if the value of $B\overline{\sigma}_{xy}$ is fairly constant, as we have every reason to expect at these high values of BR when it is mainly the hole orbits that contribute to the Hall deficit, it follows from (1) that $\overline{\rho}_{xx}/B$ passes through a maximum of $1/(2B\overline{\sigma}_{xy})$ as $\overline{\sigma}_{xx}$ rises above $\overline{\sigma}_{xy}$. On the Kohler plot of figure 16 the curve has unit gradient at this point, M, and obviously the slope below must be greater. This feature, which shows up as the hump in figure 18, is conspicuously absent from the experimental Kohler plot of Fickett, whose slope is unity at a low value of $\omega_c\tau$, where $\overline{\rho}_{xx}(B)/\rho(0) \approx 3$, but rises rather more slowly ever after. On the assumption that $\overline{\sigma}_{xy}$ cannot be far different from $0.95\ \sigma_H$, we must conclude that, unlike the theoretical curve of figure 17, in practice $\overline{\sigma}_{xx}/\sigma_H$ does not rise to cross $\overline{\sigma}_{xy}/\sigma_H$ but if anything has fallen to about $0.4\ \sigma_H$ when BR reaches 7×10^4, and this is lower than any value shown in the theoretical curves of figure 17.

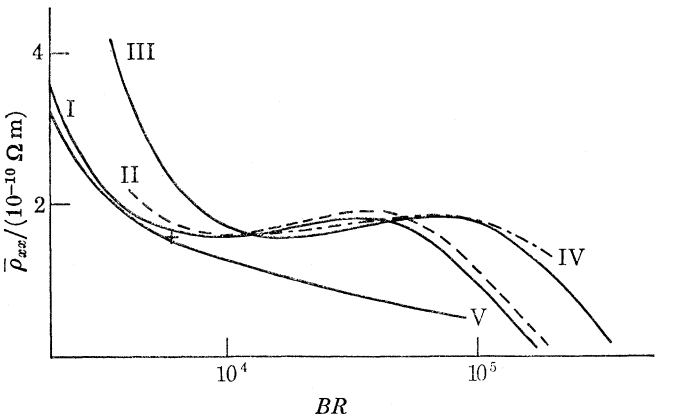

FIGURE 18. Calculations of $\overline{\rho}_{xx}$ as a function of BR. I, the same as for figures 16 and 17, i.e. $a = 1$; II, $a = 1.25$; III; $a = 2$ and longitudinal magnetoresistance doubled; IV, possible curve, shifting from I to III and beyond with increasing BR; V, experimental results of Fickett (1972). +, de Launay *et al.* (1959).

This discrepancy provides an excuse to draw attention to the many ways in which experimental conditions may fail to match the idealizations of theory, so that fair comparison is difficult to achieve. Randomness in orientation of the grains, assumed in the theory, is hardly likely to be achieved by cold drawing followed by annealing. But even if this were achieved, we still require that the grain size be considerably longer than the free path and at the same time considerably smaller than the sample diameter, for the current jetting phenomenon demands many grains in the thickness of the sample, measured along $\boldsymbol{B}$. To take this last point first, the experiments on thin plates of Martin *et al.* (1977), with many crystallites extending right through, show that when $\boldsymbol{B}$ is normal to the plate the magnetoresistance is considerably reduced. There is no evidence on the intermediate situation of a few grains within the thickness, but this hardly matters in the present case, since Fickett's samples had grain sizes of about 0.12 mm, less than one tenth of the wire diameter, and probably the thickness limitation was of little importance. On the other hand, this was achieved at the cost of grains rather smaller than the electronic free path, which in his purest samples was 0.3 mm. Since most of the scattering was almost certainly at grain boundaries, the picture we form is of virtually no scattering within the grains, and of quite considerable transparency of the boundaries, so that a typical electron would pass through two or three before being

scattered. In passing through, the electron might suffer small angle scattering, but if it did not it would find a position on the differently oriented Fermi surface having the same parallel component of wavenumber. An electron on an open or extended orbit in one grain would have a very high probability of finding itself executing a small electron orbit in the next grain, and even if it returned to the original grain it would not be to the original orbit. In a strong field, then, the grain boundary behaves very similarly to small angle scattering in terminating an extended orbit so far as $\overline{\sigma}_{xx}$ is concerned, but not for $\overline{\sigma}_{xy}$. Let us apply this to a typical good sample of Fickett's, with R equal to 7000 and a grain size of 0.12 mm. A rough estimate suggests that an open orbit with typical sinuosity should be assigned a free path (measured along the orbit) of 0.08 mm for the purpose of calculating $\overline{\sigma}_{xx}$; this is nearly four times less than the free path determined from R. In figure 17, therefore, instead of taking $\overline{\sigma}_{xx}$ where $BR = 7 \times 10^4$ we should take it where $BR = 1.8 \times 10^4$, i.e. 0.67 σ_{H} rather than 1.5 σ_{H}; but $\overline{\sigma}_{xy}$ remains at 0.95 σ_{H}. This change is enough to prevent $\overline{\sigma}_{xx}$ from increasing beyond $\overline{\sigma}_{xy}$, and so accounts for the absence of a hump in the experimental curve. It does not, however, go all the way, for we have seen that a value of 0.4 σ_{H} is needed for $\overline{\sigma}_{xx}$ to get $\overline{\rho}_{xx}$ down to Fickett's value. Figure 17 gives no hope of managing this with any model based on grain boundary effects.

The explanation is most likely to be found in the preferred orientation of grains in the drawn wires used by Fickett. According to Barrett & Massalski (1966) about 40 % would have been oriented with [100] roughly along the wire, and 60 % with [111] along the wire. Consider those grains having [100] exactly parallel, so that the transverse magnetic field lay in the (100) plane, the horizontal boundary in figure 1. There is a great wealth of periodic open orbits, but they all conduct strictly transverse to the wire, so that in spite of appearances these grains contribute very poorly indeed to $\overline{\sigma}_{xx}$; much the same goes for grains having [111] exactly parallel. It is only when the principal axes are shifted from exact parallelism with the wires that the aperiodic open orbits can play a part. It seems very reasonable, then, to suppose that the assumption of random orientation has permitted a substantial overestimate of $\overline{\sigma}_{xx}$, and that Fickett's results need not be the cause of great concern. Without a full determination of the distribution of orientations, however, it is hardly worth while embarking on the labour of computing values of $\overline{\rho}_{xx}$ for non-random arrangements.

Conclusions

In view of the attempt to explain Fickett's results in terms of non-random grain orientations, it would be naive to attach too much importance to the agreement between theory and the experiments of de Launay *et al.* It may be claimed, however, that the calculations help to dispel any lingering doubts as to the possibility of explaining the linear magnetoresistance of polycrystalline copper without invoking exotic mechanisms. Once it is recognized that the conductivity due to open and extended orbits is sufficient to raise $\overline{\sigma}_{xx}$ to a value near $\overline{\sigma}_{xy}$ and σ_{H}, the linearity follows as a simple consequence of the insensitivity of $\overline{\rho}_{xx}$ to $\overline{\sigma}_{xx}$; moreover the effective medium theory shows how the ultimately inevitable saturation of $\overline{\sigma}_{xx}$ due to the open orbits is delayed beyond the range of any experiments so far performed. To take the matter further, to the point of numerical agreement, demands measurements on very carefully characterized samples, and computation of the appropriately biased averages to allow for non-randomness of orientations. This would involve more effort, probably, than the problem deserves. A better test of the theory would be provided by the electrodeless technique, e.g. rotating a large cylinder or sphere in a transverse

PHILOSOPHICAL TRANSACTIONS OF THE ROYAL SOCIETY A MATHEMATICAL, PHYSICAL & ENGINEERING SCIENCES

field (see Delaney & Pippard 1972); if the sample were cast it would not be too hard to achieve something close to a random distribution of orientations.

It is a pleasure to acknowledge the very helpful discussions I have had with Professor J. C. Garland, and the advice and help of Mr C. M. M. Nex over computing.

References

Barrett, C. S. & Massalski, T. B. 1966 *Structure of metals*. New York: McGraw-Hill.
Delaney, J. A. & Pippard, A. B. 1972 *Rep. Prog. Phys.* **35**, 677.
Fickett, F. R. 1972 Ann. Report, Project 186, International Copper Research Association.
Halse, M. R. 1969 *Phil. Trans. R. Soc. Lond.* A **265**, 507.
Herring, C. 1960 *J. appl. Phys.* **31**, 1939.
Kapitza, P. L. 1929 *Proc. R. Soc. Lond.* A **123**, 292.
Klauder, J. R., Reed, W. A., Brennert, G. F. & Kunzler, J. E. 1966 *Phys. Rev.* **141**, 592.
Landauer, R. 1978 A.I.P. Conference Proceedings no. 40, 2.
de Launay, J., Dolecek, R. L. & Webber, R. T. 1959 *J. Phys. Chem. Solids* **11**, 37.
Lifshitz, I. M. & Peschanskii, V. G. 1958 *Zh. eksp. teor. Fiz.* **35**, 1251.
Martin, P. M., Sampsell, J. B. & Garland, J. C. 1977 *Phys. Rev.* B **15**, 5598.
Pacher, E. E. 1974 *Phys. Status Solidi* B **64**, K29.
Pippard, A. B. 1964 *Proc. R. Soc. Lond.* A **282**, 464.
Pippard, A. B 1968 *Proc. R. Soc. Lond.* A **305**, 291.
Powell, R. L. 1966 Ph.D. dissertation, University of Cambridge.
Stachowiak, H. 1970 *Physica* **45**, 481.
Stachowiak, H. 1971 *Acta phys. pol.* A **40**, 849.
Stachowiak, H. 1973 *Phys. Status Solidi* A **20**, 707.
Stratton, J. A. 1941 *Electromagnetic theory* New York: McGraw-Hill.
Strom-Olsen, J. O. 1967 *Proc R. Soc. Lond.* A **302**, 83.
Stroud, D. 1975 *Phys. Rev.* B **12**, 3368.
Ziman, J. M. 1958 *Phil. Mag.* **3**, 1117.

PHILOSOPHICAL TRANSACTIONS OF THE ROYAL SOCIETY A MATHEMATICAL, PHYSICAL & ENGINEERING SCIENCES